Atmos. Chem. Phys. Discuss., https://doi.org/10.5194/acp-2018-1088
Manuscript under review for journal Atmos. Chem. Phys.
Discussion started: 19 October 2018

Atmospheric Chemistry and Physics Discussions

The role of chlorine in tropospheric chemistry

Xuan Wang[1], Daniel J. Jacob[1,2], Sebastian D. Eastham[3], Melissa P. Sulprizio[1], Lei Zhu[1], Qianjie Chen[4], Becky Alexander[5], Tomás Sherwen[6,7], Mathew J. Evans[6,7], Ben H. Lee[5], Jessica D. Haskins[5], Felipe D. Lopez-Hilfiker[8], Joel A. Thornton[5], Gregory L. Huey[9], and Hong Liao[10]

[1] School of Engineering and Applied Sciences, Harvard University, Cambridge, Massachusetts, USA
[2] Department of Earth and Planetary Sciences, Harvard University, Cambridge, Massachusetts, USA
[3] Laboratory for Aviation and the Environment, Massachusetts Institute of Technology, Cambridge, Massachusetts, USA
[4] Department of Chemistry, University of Michigan, Ann Arbor, Michigan, USA
[5] Department of Atmospheric Sciences, University of Washington, Seattle, USA
[6] Wolfson Atmospheric Chemistry Laboratories, Department of Chemistry, University of York, York, UK
[7] National Centre for Atmospheric Science, University of York, York, UK
[8] Paul Scherrer Institute, Villigen, Switzerland
[9] School of Earth and Atmospheric Science, Georgia Institute of Technology, Atlanta, GA, USA
[10] School of Environmental Science and Engineering, Nanjing University of Information Science and Technology, Nanjing, China

Correspondence to: Xuan Wang (wangx@seas.harvard.edu)

Abstract. We present a comprehensive simulation of tropospheric chlorine within the GEOS-Chem global 3-D model of oxidant-aerosol-halogen atmospheric chemistry. The simulation includes explicit accounting of chloride mobilization from sea-salt aerosol by acid displacement of HCl and by other heterogeneous processes. Additional sources of tropospheric chlorine (combustion, organochlorines, transport from stratosphere) are small in comparison. Reactive gas-phase chlorine Cl*, including Cl, ClO, Cl_2, BrCl, ICl, HOCl, $ClNO_3$, $ClNO_2$, and minor species, is produced by the HCl + OH reaction and by heterogeneous conversion of sea-salt aerosol chloride to BrCl, $ClNO_2$, Cl_2, and ICl. The model simulates successfully the observed mixing ratios of HCl in marine air (highest at northern mid-latitudes) and the associated HNO_3 decrease from acid displacement. It captures the high $ClNO_2$ mixing ratios observed in continental surface air at night with chlorine of sea salt origin transported inland as HCl and fine aerosol. It simulates successfully the vertical profiles of HCl measured from aircraft, where enhancements in the continental boundary layer can again be explained by transport inland of the marine source. It does not reproduce the boundary layer Cl_2 mixing ratios measured in the WINTER aircraft campaign (1-5 ppt in the daytime, low at night); the model is too high at night compared to WINTER observations, which could be due to uncertainty in the rate of the $ClNO_2$ + Cl^- reaction, but we have no explanation for the daytime observations. The global mean tropospheric concentration of Cl atoms in the model is 620 cm^{-3} and contributes 1.0% of the global oxidation of methane, 20% of ethane, 14% of propane, and 4% of methanol. Chlorine chemistry increases global mean tropospheric BrO by 85%, mainly through the HOBr + Cl^- reaction, and decreases global burdens of tropospheric ozone by 7% and OH by 3%

Atmos. Chem. Phys. Discuss., https://doi.org/10.5194/acp-2018-1088
Manuscript under review for journal Atmos. Chem. Phys.
Discussion started: 19 October 2018

through the associated bromine radical chemistry. $ClNO_2$ chemistry drives increases in ozone of up to 8 ppb over polluted continents in winter.

1 Introduction

Mobilization of chloride (Cl^-) from sea salt aerosol (SSA) is a large source of chlorine gases to the troposphere (Graedel and Keene, 1995; Finlayson-Pitts, 2003). These gases may generate chlorine radicals with a broad range of implications for tropospheric chemistry including the budgets of ozone, OH (the main tropospheric oxidant), volatile organic compounds (VOCs), nitrogen oxides, other halogens, and mercury (Saiz-Lopez and von Glasow, 2012; Simpson et al., 2015). Only a few global models have attempted to examine the implications of tropospheric chlorine chemistry (Singh and Kasting, 1988; Long et al., 2014; Hossaini et al., 2016) and then only with a limited representation of processes. Here we present a more comprehensive analysis of this chemistry within the framework of the GEOS-Chem chemical transport model (CTM).

Saiz-Lopez and Glasow (2012) and Simpson et al. (2015) present recent reviews of tropospheric halogen chemistry including chlorine. Sea-salt aerosols represent a large chloride flux to the atmosphere but most of that chloride is removed rapidly by deposition. Only a small fraction is mobilized to the gas phase as HCl or other species. Additional minor sources of tropospheric chlorine include open fires, coal combustion, waste incineration, industry, road salt application, and ocean emission of organochlorine compounds (McCulloch et al., 1999; Lobert et al., 1999; WMO, 2014; Kolesar et al. 2018). It is useful to define Cl_y as total gas-phase inorganic chlorine, excluding particle phase Cl^- . Most of this Cl_y is present as HCl, which is removed rapidly by deposition but also serves as a source of chlorine radicals. Rapid cycling takes place between the chlorine radicals and other chlorine gases, eventually returning HCl. Thus it is useful to define reactive chlorine Cl* as the ensemble of Cl_y gases other than HCl.

Cycling of chlorine affects tropospheric chemistry in a number of ways (Finlayson-Pitts, 2003; Saiz-Lopez and von Glasow, 2012). Acid displacement of Cl^- by nitric acid (HNO_3) is a source of NO_3^- aerosol (Massucci et al., 1999). Cl atoms provide a sink for methane, other volatile organic compounds (VOCs) (Atkinson, 1997), and dimethyl sulfide (DMS) (Hoffmann et al., 2016; Chen et al., 2018). Cycling between Cl radicals drives catalytic ozone loss, and converts nitrogen oxide radicals ($NO_x \equiv NO + NO_2$) to HNO_3, decreasing both ozone and OH. On the other hand, mobilization of Cl^- by N_2O_5 in polluted environments produces $ClNO_2$ radicals that photolyze in the daytime to stimulate ozone production (Behneke et al., 1997; Osthoff et al., 2008). Chlorine also interacts with other halogens (bromine, iodine), initiating further radical chemistry that affects ozone, OH, and mercury.

A number of global modeling studies have investigated tropospheric halogen chemistry but most have focused on bromine and iodine, which are more active than chlorine because of the lower chemical stability of HBr and HI (Parrella et al., 2012; Sherwen et al., 2016a). Interest in global modeling of tropospheric chlorine has focused principally on quantifying the Cl

atom concentration as a sink for methane (Keene et al., 1990; Singh et al., 1996). Previous global 3-D models found mean tropospheric Cl atom concentrations of the order of 10^3 cm^{-3}, with values up to 10^4 cm^{-3} in the marine boundary layer (MBL), and contributing 2-3% of atmospheric methane oxidation (Long et al, 2014; Hossaini et al., 2016; Schmidt et al., 2016; Sherwen et al., 2016b). A regional modeling study by Sawar et al. (2014) included $ClNO_2$ chemistry in a standard ozone mechanism and found increases in surface ozone mixing ratios over the US of up to 7 ppb (ppb = nmol/mol).

Here we present a more comprehensive analysis of global tropospheric chlorine chemistry and its implications, building on previous model development of tropospheric oxidant-aerosol-halogen chemistry in GEOS-Chem. A first capability for modeling tropospheric bromine GEOS-Chem was introduced by Parrella et al. (2012). Eastham et al. (2014) extended it to describe stratospheric halogen chemistry including chlorine and bromine cycles. Schmidt et al. (2016) updated the tropospheric bromine simulation to include a broader suite of heterogeneous processes, and extended the Eastham et al. (2014) stratospheric chlorine scheme to the troposphere. Sherwen et al. (2016a; b) added iodine chemistry and made further updates to achieve a consistent representation of tropospheric chlorine-bromine-iodine chemistry in GEOS-Chem. Chen et al. (2017) added the aqueous-phase oxidation of SO_2 by HOBr and found a large effects on the MBL bromine budget. Our work advances the treatment of tropospheric chlorine in GEOS-Chem to include in particular a consistent treatment of SSA chloride and chlorine gases, SSA acid displacement thermodynamics, improved representation of heterogeneous chemistry, and better accounting of chlorine sources. We evaluate the model with a range of global observations for chlorine and related species. From there we quantify the global tropospheric chlorine budgets, describe the principal chemical pathways, and explore the impacts on tropospheric chemistry.

2 Model description

2.1 GOES-Chem model with Cl+Br+I halogen chemistry

We build our new tropospheric chlorine simulation capability onto the standard version 12.0.0 of GEOS-Chem (http://www.geos-chem.org). The standard version includes a detailed tropospheric oxidant-aerosol-halogen mechanism as described by Sherwen et al. (2016b) and Chen et al. (2017). It includes 12 gas phase Cl_y species: Cl, Cl_2, Cl_2O_2, $ClNO_2$, $ClNO_3$, ClO, ClOO, OClO, BrCl, ICl, HOCl, and HCl. It allows for heterogeneous chemistry initiated by SSA Cl^- but does not actually track the SSA Cl^- concentration and its exchange with gas-phase Cl_y. Here we add two new transported reactive species to GEOS-Chem to describe Cl^- aerosol, one for the fine mode (< 1μm diameter) and one for the coarse mode (> 1μm diameter). The standard GEOS-Chem wet deposition schemes for aerosols (Liu et al., 2001) and gases (Amos et al., 2012) are applied to Cl^- aerosol and Cl_y gases respectively, the latter with Henry's law constants from Sander (2015). Dry deposition of Cl^- aerosol follows that of SSA (Jaeglé et al., 2012), and dry deposition of Cl_y gases follows the resistance-in-series scheme of Wesely (1989) as implemented in GEOS-Chem by Wang et al. (1998). We also add to the model two SSA alkalinity tracers in the fine and coarse modes, and retain the inert SSA tracer to derive local concentrations of non-volatile

cations (Section 2.3). SSA debromination by oxidation of Br^- as described by Schmidt et al. (2016) was not included in standard version 12.0.0 of GEOS-Chem because of concern over excessive MBL BrO (Sherwen et al., 2016b), but Zhu et al. (2018) show that it allows in fact a successful simulation of MBL BrO to compensate for losses from aqueous-phase oxidation of SO_2 by HOBr (Chen et al., 2017) and oxidation of marine acetaldehyde by Br atoms (Millet et al., 2010). We include it in this work.

We present a 1-year global simulation for 2016 driven by GEOS-FP (forward processing) assimilated meteorological fields from the NASA Global Modeling and Assimilation office (GMAO) with native horizontal resolution of 0.25° × 0.3125° and 72 vertical levels from the surface to the mesosphere. Our simulation is conducted at 4° × 5° horizontal resolution and meteorological fields are conservatively regridded for that purpose. Stratospheric chemistry is represented using 3-D monthly mean production rates and loss rate constants from a fully coupled stratosphere-troposphere GEOS-Chem simulation (Murray et al., 2012; Eastham et al., 2014).

2.2 Sources of chlorine

Table 1 lists the global sources and sinks of tropospheric gas-phase inorganic chlorine (Cl_y) and reactive chlorine (Cl*) in our model. Both are dominated by mobilization of Cl^- from SSA. SSA emission is computed locally in GEOS-Chem as integrals of the size-dependent source function over two size bins, fine (0.2-1 μm diameter) and coarse (1-8 μm diameter). The source function depends on wind speed and sea surface temperature (Jaegle et al., 2010). We obtain a global SSA source of 3230 Tg a^{-1} for 2016 or 1780 Tg a^{-1} Cl^- (assuming fresh SSA to be 55.05% Cl^- by mass; Lewis and Schwartz, 2004). Only 64 Tg Cl^- a^{-1} (3.6%) is mobilized to Cl_y by acid displacement and other heterogeneous reactions, while the rest is deposited. 42% of the mobilization is from fine SSA and 58% is from coarse SSA. Details of this mobilization are in Sections 2.3 and 2.4. 80% of the mobilization is by acid displacement to HCl, which is in turn efficiently deposited. Only 19% of HCl is further mobilized to Cl* by reaction with OH to drive chlorine radical chemistry. Direct generation of Cl* from SSA through heterogeneous chemistry provides a Cl* source of comparable magnitude to HCl + OH, with dominant contributions from HOBr + Cl^- and N_2O_5 + Cl^- (the latter in polluted high-NO_x environments).

Cl* can also be produced in the model by atmospheric degradation of the organochlorine gases CH_3Cl, CH_2Cl_2, $CHCl_3$, and CH_2ICl. These gases are mainly of biogenic marine origin, with the exception of CH_2Cl_2 which has a large industrial solvent source (Simmonds et al., 2006). Mean tropospheric lifetimes are 520 days for CH_3Cl, 280 days for CH_2Cl_2, 260 days for $CHCl_3$, and 0.4 days for CH_2ICl. Emissions of CH_3Cl, CH_2Cl_2, and $CHCl_3$ are implicitly treated in the model by specifying monthly mean surface air boundary conditions in 5 latitude bands (60-90°N, 30-60°N, 0-30°N, 0-30°S, and 30-90°S) from AGAGE observations (Prinn et al., 2016). Emission of CH_2ICl is from Ordóñez et al. (2012), as described by Sherwen et al. (2016a). Tropospheric oxidation of hydrochlorofluorocarbons (HCFCs) is neglected as a source of Cl* because it is small compared to the other organochlorines. The stratospheric source of Cl_y from HCFCs, chlorofluorocarbons (CFCs), and CCl_4

is included in the model on the basis of the Eastham et al. (2014) GEOS-Chem stratospheric simulation as described in Section 2.1. Tropospheric organochlorines give a global Cl* source of 3. 3 Tg Cl a^{-1} in Table 1, smaller than that from heterogeneous SSA Cl^- reactions (11.9 Tg Cl a^{-1}) or oxidation of HCl by OH (9.7 Tg Cl a^{-1}). The stratosphere is a minor global source of tropospheric Cl* (0.06 Tg Cl a^{-1}) although it could be important in the upper troposphere (Schmidt et al., 2016).

We also include primary HCl emissions from open fires. We apply the emission factors of ($HCl+Cl^-$) from Lobert et al. (1999) for different vegetation types to the GFED4 (Global Fire Emissions Database) biomass burned inventory (van der Werf et al., 2010; Giglio et al., 2013), resulting in a global source of 7.6 Tg Cl a^{-1} emitted as HCl.

Anthropogenic sources of HCl include coal combustion, waste incineration, and industrial activities. The only global emission inventory is that of McCulloch et al. (1999), which gives a total of 6.7 Tg Cl a^{-1}. As shown in Section 4.2, we find that this greatly overestimates atmospheric observations of HCl over the US. National inventories of HCl from coal combustion available for China (236 Gg Cl a^{-1} in 2012; Liu et al., 2018) and the US (69 Gg Cl a^{-1} in 2014; US EPA, 2018) are respectively six and seven times lower than McCulloch et al. (1999) for those countries. We choose therefore not to include anthropogenic HCl emissions in our standard simulation, as they are small in any case from a global budget perspective. We show in Section 4.2 that we can account for HCl observations in continental air largely on the basis of the SSA Cl^- source. We also do not consider Cl* generation from snow/ice surfaces which could be important in the Arctic spring MBL (Liao et al., 2014) but is highly uncertain and would only affect a small atmospheric domain.

2.3 HCl/Cl^- acid displacement thermodynamics

SSA Cl^- can be displaced to HCl by strong acids (H_2SO_4, HNO_3) once the initial supply of SSA alkalinity (≡ HCO_3^- + $2\times CO_3^{2-}$) has been exhausted. The acid displacement is described by

$$Cl^- + HNO_3 \rightleftarrows HCl + NO_3^- \qquad \text{(R1)}$$

$$Cl^- + H_2SO_4 \rightleftarrows HCl + HSO_4^- \qquad \text{(R2)}$$

(R1) must be treated as an equilibrium because HNO_3 and HCl have comparable effective Henry's law constants (Jacob et al.,, 1985). H_2SO_4 has a much lower vapor pressure so that (R2) fully displaces HCl. Additional displacement of HCl by HSO_4^- does not take place because HSO_4^- is a much weaker acid than HCl (Jacob et al., 1985).

Alkalinity initially prevents any acid displacement in freshly emitted SSA. Alkalinity is emitted as 0.07 mole equivalents per kg of dry SSA, and is transported in the model as two separate tracers for fine and coarse SSA. It is consumed over time by uptake of acids (SO_2, H_2SO_4, HNO_3, and HCl) as described by Alexander et al. (2005), and once fully consumed it is set to zero (titration). The SSA is then diagnosed as acidified, enabling acid displacement by (R1)-(R2). In our simulation,

Atmos. Chem. Phys. Discuss., https://doi.org/10.5194/acp-2018-1088
Manuscript under review for journal Atmos. Chem. Phys.
Discussion started: 19 October 2018

alkalinity is titrated everywhere shortly after emission except in some areas of the Southern Ocean, which is consistent with the model results of Alexander et al. (2005) and Kasibhatla et al. (2018).

Observations in the MBL indicate that fine SSA is usually internally mixed with sulfate-nitrate-ammonium (SNA) aerosols while coarse SSA is externally mixed (Fridlind and Jacobson, 2000; Dasgupta et al., 2007). Acid displacement for the acidified fine SSA is thus computed by adding HCl/Cl^- to the SNA thermodynamics. The local thermodynamic gas-aerosol equilibrium for the resulting H_2SO_4-HCl-HNO_3-NH_3-NVC system is calculated with ISORROPIA II (Fountoukis and Nenes, 2007). The calculation is done assuming an aqueous aerosol even if relative humidity is below the deliquescence point (metastable state). NVC (non-volatile cations) describes the sum of cations emitted as SSA and is treated in ISORROPIA II using Na^+ as proxy. Here NVC is emitted as 16.4 moles equivalent per kg of dry SSA to balance the emission of SSA anions including Cl^- , alkalinity, and sea-salt sulfate. The NVC concentration is determined locally from the mass concentration of the inert SSA tracer.

Acid displacement for acidified coarse SSA is assumed to be driven by uptake of strong acids from the gas phase, mainly HNO_3 (Kasibhatla et al., 2018). The ISORROPIA II calculation is conducted with 2 gas species (HNO_3 and HCl) and 4 aerosol species (NVC, Cl^-, SO_4^{2-}, and NO_3^-). Here the sulfate includes only the emitted sea-salt component and that produced by heterogeneous SO_2 oxidation in coarse SSA (Alexander et al., 2005). In the case of coarse aerosols, there may be significant mass transfer limitation to reaching gas-aerosol thermodynamic partitioning (Meng and Seinfeld, 1996). To account for this limitation, the concentrations are adjusted after the ISORROPIA II calculation following the dynamic method of Pilinis et al. (2000). This 2-step thermodynamics approach has been used in previous studies (Koo et al., 2003; Kelly et al., 2010).

2.4 Heterogeneous chemistry of Cl^-

Table 2 lists the heterogeneous reactions of Cl^- other than acid displacement. The loss rate of a gas species X due to reaction with Cl^- is calculated following Jacob (2000):

$$\frac{dn_X}{dt} = -\left(\frac{r}{D_g} + \frac{4}{c\gamma([Cl^-])}\right)^{-1} An_X \qquad (1)$$

Here n_X is the number density of species X (molecules of X per unit volume of air), A is the aerosol or cloud surface area concentration per unit volume of air, r is the effective particle radius, D_g is the gas-phase molecular diffusion coefficient of X, c is the average gas-phase thermal velocity of X, and γ is the reactive uptake coefficient which is a function of the aqueous-phase molar Cl^- concentration [Cl^-] (moles of Cl^- per liter of water). Values of γ in Table 2 are mostly from recommendations by the International Union of Pure and Applied Chemistry (IUPAC) (Ammann et al., 2013).

Atmos. Chem. Phys. Discuss., https://doi.org/10.5194/acp-2018-1088
Manuscript under review for journal Atmos. Chem. Phys.
Discussion started: 19 October 2018

The heterogeneous reactions take place in both clear-air aerosol and clouds. The GEOS-FP input meteorological data include cloud fraction and liquid/ice water content for every grid cell. Concentrations per cm^3 of air of aerosol-phase species (including fine and coarse Cl^- and Br^-) within a grid cell are partitioned between clear air and cloud as determined by the cloud fraction. Clear-air aqueous-phase concentrations for use in calculating heterogeneous reaction rates are derived from the RH-dependent liquid water contents of fine and coarse SSA using aerosol hygroscopic growth factors from the Global Aerosol Database (GADS, Koepke et al., 1997) with update by Lewis and Schwartz (2004). In-cloud aqueous-phase concentrations are derived using liquid and ice water content from the GEOS-FP meteorological data. Values of *r* in equation (1) are specified as RH-dependent effective radii for the different clear-air aerosol components (Martin et al., 2002), and are set to 10 μm for cloud droplets and 75 μm for ice particles. These effective radii are also used to infer the area concentrations *A* on the basis of the mass concentrations. Heterogeneous chemistry in ice clouds is restricted to the unfrozen layer coating the ice crystal, which is assumed to be 1% of the ice crystal radius (Schmidt et al., 2016).

The reactions of HOBr, HOCl, and $ClNO_2$ with Cl^- in Table 2 are pH-dependent and require acidic conditions (Abbatt and Waschewsky, 1998; Fickert et al., 1999). They are considered only when SSA alkalinity has been titrated. The pH of Cl^- containing fine aerosol after alkalinity has been titrated is calculated by ISORROPIA II. Liquid cloud water pH is calculated in GEOS-Chem following Alexander et al. (2012), with update to include Cl^- and NVC. Coarse mode SSA and ice cloud pH are assumed to be 5 and 4.5 respectively (Schmidt et al., 2016).

3 Global budget and distribution of tropospheric chlorine

Figure 1 describes the global budget and cycling of tropospheric inorganic chlorine in GEOS-Chem. The dominant source of Cl_y is acid displacement from SSA. The global rate of Cl_y generation from acid displacement is 52 Tg Cl a^{-1}, close to the observationally based estimate of 50 Tg Cl a^{-1} by Graedel and Keene (1995), and lower than the model estimate of 90 Tg Cl a^{-1} from Hossaini et al. (2016), who treated displacement of Cl^- by HNO_3 as an irreversible rather than thermodynamic equilibrium process. HCl is the largest reservoir of Cl_y in the troposphere, with a global mean tropospheric mixing ratio of 60 ppt (ppt = pmol/mol).

Acid displacement generates Cl_y as HCl, which is mostly removed by deposition. Broader effects of chlorine on tropospheric chemistry take place through the cycling of radicals originating from production of reactive chlorine $Cl^* \equiv Cl_y - HCl$. HCl contributes 10 Tg Cl a^{-1} to Cl* through the reaction between HCl and OH. Beside this source, Cl^- provides a Cl* source of 12 Tg Cl a^{-1} through heterogeneous reactions with principal contributions from HOBr + Cl^- (8.6 Tg Cl a^{-1}) and N_2O_5 + Cl^- (1.8 Tg Cl a^{-1}). This heterogeneous source of 12 Tg Cl a^{-1} is much higher than previous estimates of 5.6 Tg Cl a^{-1} (Hossaini et al., 2016) and 6.1 Tg Cl a^{-1} (Schmidt et al., 2016). Schmidt et al. (2016) only considered the HOBr + Cl^- reaction. Production of the chlorine radicals Cl and ClO is contributed by the HCl +OH reaction (45%) and by photolysis of BrCl (40%), $ClNO_2$

(8%), Cl_2 (4%), and ICl (2%). Loss of Cl* is mainly through the reaction of Cl with methane (46%) and other organic compounds (CH_3OH 15%, CH_3OOH 11%, C_2H_6 8%, higher alkanes 8%, and CH_2O 7%).

Conversion of Cl to ClO* drives some cycling of chlorine radicals, but the associated chain length versus Cl* loss is short ($4.1x10^4/2.5x10^4 = 1.6$). Conversion of Cl to ClO is mainly by reaction with ozone (98%), while conversion of ClO back to Cl is mostly by reaction with NO (72%), driving a null cycle as NO_2 photolyzes to regenerate NO and ozone.

Figure 2 shows the annual mean global distributions of HCl mixing ratios and Cl atom concentrations. The mixing ratio of HCl decreases from the surface to the middle troposphere, reflecting the sea salt source, and then increases again in the upper troposphere where it is supplied by transport from the stratosphere and has a long lifetime due to lack of scavenging. Remarkably, Cl atom number densities show little decrease with altitude, contrary to the common assumption that tropospheric Cl atoms should be mainly confined to the MBL where the SSA source resides (Singh et al., 1996). We find that the effect of the SSA source is offset by the slower sink of Cl* at higher altitudes due to the strong temperature dependence of the reactions between Cl atom and organic compounds. Transport of HCl and Cl* from the stratosphere also contribute to the source of Cl atoms in the upper troposphere.

HCl mixing ratios in marine surface air are usually highest along polluted coastlines where the large sources of HNO_3 and H_2SO_4 from anthropogenic NO_x and SO_2 emissions drive acid displacement from SSA. By contrast, HCl mixing ratios over the Southern Ocean are low because of the low supply of acid gases. The distribution of Cl atoms in surface air reflects its sources from both HCl +OH and the heterogeneous production of Cl*. The highest concentrations are in northern Europe due to production of $ClNO_2$ from the N_2O_5 + Cl^- reaction (R3). Cl atom concentrations in marine air are shifted poleward relative to HCl because of increasing bromine radical concentrations (Parrella et al., 2012), driving BrCl formation by the HOBr + Cl^- reaction (R5).

Figure 3 shows the global mean vertical distributions of reactive chlorine species (Cl*) in continental and marine air. Mean boundary layer mixing ratios are higher over land than over the ocean because of the $ClNO_2$ source from N_2O_5 +Cl^- in high-NO_x polluted air (Thornton et al., 2010). $ClNO_2$ mixing ratios are much higher than in the Sherwen et al. (2016b) model which restricted its production in SSA, reflecting the importance of HCl dissolved in SNA aerosol which allows further transport inland. High mixing ratios of $ClNO_3$ in the upper troposphere are due to transport from the stratosphere and inefficacy of the sinks from hydrolysis and heterogeneous chemistry. Over the oceans in the MBL we find comparable contributions from HOCl (mainly in daytime) and Cl_2 and $ClNO_2$ (mainly at night). The BrCl mixing ratio is much lower than in the previous model studies of Long et al. (2014) and Sherwen et al. (2016b) which had very large sources from the HOBr + Cl^- reaction (R5). Our lower BrCl mixing ratio is due to competition from the HOBr + S(IV) reaction (Chen et al., 2017) and to oceanic VOC emissions (Millet et al., 2010), both of which act to depress bromine radical concentrations in the MBL (Zhu et al., 2018).

Atmos. Chem. Phys. Discuss., https://doi.org/10.5194/acp-2018-1088
Manuscript under review for journal Atmos. Chem. Phys.
Discussion started: 19 October 2018

4 Comparison to observations

Here we compare the model simulation for 2016 to available observations for gas-phase chlorine and related species collected in different years. Although the meteorological years are different, we expect inter-annual variability to be a minor factor in model error. Previous evaluation of the GEOS-Chem sea salt source by Jaeglé et al. (2011) showed general skill in simulating SSA observations and we do not repeat this evaluation here.

4.1 Surface air observations

Table 3 compares our simulated Cl^- SSA deficits to an ensemble of marine air observations compiled by Graedel and Keene (1995). The Cl^- deficit is relative to seawater composition and provides an indicator of the mobilization of Cl^- through acid displacement and heterogeneous chemistry. The observations show a wide range from -50% to +90%, and Graedel and Keene (1995) emphasized that uncertainties are large. Slight negative deficits in the observations could be caused by titration of alkalinity by HCl but large negative deficits are likely due to error. Mean model deficits sampled for the regions and months of the observations range from +4% to +40%, not inconsistent with the observations. The largest model deficits are in polluted coastal regions because of acid displacement and this also where the measured deficits are largest.

Figure 4 compares simulated HCl and HNO_3 mixing ratios to concurrent observations of both gases at coastal sites and over oceans. Mean HCl mixing ratios average 323 ± 155 ppt in the model and 347 ± 227 ppt in the observations for the ensemble of regions. The HCl mixing ratios in the model are mainly from acid displacement from SNA. A sensitivity simulation without acid displacement from SSA has less than 7 ppt HCl in all regions. The model also captures the spatial variability of the mean HCl mixing ratios across locations (r = 0.88), which largely reflects the HCl enhancement at polluted coastal sites and northern mid-latitudes (Figure 2). Simulated HNO_3 mixing ratios average 190 ± 255 ppt across locations as compared to 137 ± 151 ppt in the observations, again with good simulation of spatial variability (r = 0.96) driven by NO_x emissions. HNO_3 mixing ratios are sensitive to acid displacement from SSA, as the sensitivity simulation without acid displacement shows mean values of 441 ± 361 ppt that are much higher than observed. This could partly explain the general problem of models overestimating HNO_3 in remote air (Bey et al., 2001).

A number of surface air measurements have been made of Cl^* as the water-soluble component of Cl_y after removal of HCl (Keene et al., 1990), although most of these measurements are below the detection limit (Table 4, mostly from Keene et al. (2009)). This Cl* has been commonly assumed to represent the sum of Cl_2 and HOCl (Pszenny et al., 1991) but it would also include $ClNO_2$, $ClNO_3$, and minor components of Cl*. Table 4 shows that simulated Cl* mixing ratios are consistent with the measurements to the extent that comparison is possible. Simulated Cl* over remote oceans is dominated by HOCl, but $ClNO_2$ is responsible for the high values over the Atlantic Ocean near Europe.

Lawler et al. (2010) measured HOCl and Cl_2 mixing ratios at Cape Verde for 7 days in June 2009. Daytime HOCl and nighttime Cl_2 mixing ratios ranged 40-200 ppt and 5-40 ppt respectively during the first 3 days, and dropped to 0-20 ppt and 0-5 ppt during the last 4 days. The first 3 days were affected by transport from northern Africa, while the last 4 days sampled background marine air. Our simulated daytime HOCl and nighttime Cl_2 mixing ratios for that site and month are ~5ppt and ~0.3ppt respectively, with little day-to-day variability and consistent with the last 4 days of observations. We have no explanation for the high values observed on the first 3 days.

Because of the strong diurnal variations and spikiness in $ClNO_2$, peak values are usually reported instead of means in the observations. Table 5 shows a comparison of peak $ClNO_2$ mixing ratios between the model and available surface $ClNO_2$ observations. Many of these reported values were from short plumes lasting a few minutes, which are difficult for the model to produce due to its coarse resolution and hourly diagnostic period. However, we find that the model does credibly in capturing the magnitude of observations. The previous GEOS-Chem simulation of Sherwen et al. (2016b) only considered $ClNO_2$ production in SSA and as a result their $ClNO_2$ mixing ratios were consistently below a few ppt at continental sites (e.g., Calgary and Boulder in Table 5). Our simulation can reproduce the observed >100 ppt concentrations at these sites because it accounts for HCl dissolved in SNA aerosol, allowing marine influence to extend further inland.

4.2 Comparison to aircraft measurements

The WINTER aircraft campaign over the eastern US and offshore in February-March 2015 provides a unique data set for evaluating our model. Measurements included HCl, Cl_2, $ClNO_2$, $ClNO_3$, and HOCl by Time of Flight Chemical Ionization Mass Spectrometry (TOF-CIMS) (Lee et al., 2018). We focus on measurements of HCl, Cl_2, $ClNO_2$, and HOCl because calibration for $ClNO_3$ needs further examination. The WINTER-mean 1s detection limits for HCl, $ClNO_2$, HOCl, and Cl_2 were 100, 2, 2, and 1 ppt respectively (Lee et al., 2018). The estimated calibration uncertainty for the reported data is ±30% for all chlorine species, for which direct calibrations were performed, and the uncertainty represents a conservative estimate of the variability in measured sensitivity. As discussed in Lee et al. (2018), labeled 15-N_2O_5 was added to the inlet tip during WINTER flights to quantify inlet production of $ClNO_2$, which was found to be negligible (<<10% of measured $ClNO_2$), but inlet production of Cl_2, for example, from surface reactions of HOCl with adsorbed HCl, was not evaluated.

Figure 5 compares the observed median vertical profiles of HCl, $ClNO_2$, HOCl, and Cl_2 in WINTER to the model sampled along the flight tracks for the corresponding period. Figure 6 compares the median diurnal variations below 1 km altitude, separately over ocean and land. We exclude daytime (10:00-16:00 local) data for $ClNO_2$ in Figure 5 because its mixing ratios are near-zero (Figure 6).

The WINTER observations of HCl show median values of 380 ppt near the surface, dropping to a background of 100-200 ppt in the free troposphere (Figure 5). The model matches the observations in the lowest 2 km but its free tropospheric background is lower. As shown in Figure 6, HCl mixing ratios in the lowest km average 60% higher over ocean than over

land in both the observations and the model, reflecting the marine source. There is no significant diurnal cycle of HCl, either in the model or the observations, reflecting its long lifetime. The aircraft did not sample the nighttime continental surface layer where HCl depletion by dry deposition could occur.

Also shown in Figure 5 is a sensitivity simulation including anthropogenic HCl emissions from McCulloch et al. (1999) as described in Section 2.2. The resulting model mixing ratios are too high. In fact, as shown in Figure 6, we can simulate successfully the continental boundary layer observations of HCl in WINTER by invoking SSA as the only significant source of chlorine. Even though coarse SSA is rapidly deposited during transport inland, HCl can be transported further through its equilibrium with fine-mode SNA aerosol.

Similar results are found in Figure 7 when comparing the model to HCl vertical profiles measured by the Georgia Tech CIMS instrument during the SEAC^{4}RS campaign over the Southeast US in August-September 2013 (Toon et al., 2016) and the KORUS-AQ campaign over and around the Korea peninsula in May-June 2015. For SEAC^{4}RS we only consider the Southeast US domain as in Kim et al. (2015). The standard model simulation without anthropogenic chlorine successfully simulates the boundary layer HCl observations, but adding the McCulloch et al. (1999) anthropogenic inventory results in large overestimates. Boundary layer HCl mixing ratios over land are much lower in SEAC^{4}RS than in WINTER and this is well reproduced by the model, where the difference is due to seasonal contrast in the SSA source and in the inflow of marine air. The free tropospheric background observed in SEAC^{4}RS and KORUS-AQ data is only ~25 ppt, much lower than in WINTER (100-200 ppt), whereas the model free tropospheric background is consistently 20-50 ppt in all three campaigns. The free tropospheric background in WINTER is difficult to compare as the observations are near the stated detection limits, estimated at 100 ppt, driven not by counting statistics but by overlap of the mass spectral peak for HCl by a water dimer, elevated due to the intentional addition of water vapor to the ionization region (Lee et al 2018).

Mixing ratios of $ClNO_2$ observed during the WINTER campaign are above the detection limit only in the lowest km of atmosphere at night, and are much higher over the ocean than over land. This is well simulated by the model (Figures 5 and 6), and reflects for the sources from SSA heterogeneous chemistry combined with the fast loss by photolysis in daytime. At night, the model matches well the observed $ClNO_2$ mixing ratios but greatly overestimates Cl_2. We find that model Cl_2 in WINTER is high because of the large source from the $ClNO_2$ + Cl^- reaction:

$$ClNO_2 + Cl^- \rightarrow NO_2^- + Cl_2 \qquad \text{(R7)}$$

This reaction provides only 38% of the global model source of Cl_2 (Figure 1) but it completely dominates during WINTER. The reactive uptake coefficient for (R7) is based on a single laboratory study (Roberts et al., 2008). A sensitivity simulation without this reaction (dashed red lines in Figure 6) can reproduce the low Cl_2 mixing ratios observed over the ocean at night. Further studies are needed to better understand this reaction.

The model underestimates both observed HOCl and Cl_2 at daytime, over the ocean as well as over land. These species have short lifetimes against photolysis (less than a few minutes). Direct anthropogenic emission from coal combustion has been proposed (Chang et al., 2002) but would only be observed in plumes and not over the oceans. Matching the >1 ppt Cl_2 observed during daytime is particularly problematic since it would require a large photochemical source absent from the model. Lawler et al. (2011) suggested a fast daytime HOCl source from a hypothetical light-dependent Cl^- oxidation. The measurements of Cl_2 are also possibly subject to positive artifact from rapid heterogeneous conversion of chlorine species on the surface of the TOF-CIMS inlet, see above (Lee et al., 2018).

5 Global implications of tropospheric chlorine chemistry

5.1 Cl atom and its impact on VOCs

The global mean pressure-weighted tropospheric Cl atom concentration in our simulation is 620 cm^{-3}, while the MBL concentration averages 1200 cm^{-3} (Figure 2). Our global mean is lower than the previous global model studies of Hossaini et al. (2016) (1300 cm^{-3}) and Long et al. (2014) (3000 cm^{-3}), which had excessive Cl* generation as discussed above. It is consistent with the upper limit of 1000 cm^{-3} inferred by Singh et al. (1996) from global modeling of C_2Cl_4 observations (C_2Cl_4 is highly reactive with Cl atoms). Isotopic observations of methane have been used to infer a Cl atom concentration in the MBL higher than 9000 cm^{-3} in the extra-tropical Southern Hemisphere (Lowe et al., 1999; Platt et al., 2004; Allen et al., 2007), much higher than our estimate of 800 cm^{-3} over this region. More recently, Gromov et al. (2018) revisited these data together with added constraints from CO isotope measurements and concluded that extra-tropical Southern Hemisphere concentrations of Cl atoms in the MBL should be lower than 900 cm^{-3}, consistent with our estimate.

Tropospheric oxidation by Cl atoms drives a present-day methane loss rate of 5.3 Tg a^{-1} in our model, contributing 1.0% of total methane chemical loss. This is a small effect considering the 10% current uncertainty in the overall atmospheric lifetime of methane (Prather et al., 2012). Zhang et al. (2018) suggested that satellite observations of the global distribution of atmospheric methane could be used to independently constrain methane sources and the dominant sink from oxidation by tropospheric OH. The distribution of the methane loss rate due to Cl atoms is shown in Figure 8. The general latitudinal and seasonal patterns are not sufficiently different from OH (shown in Zhang et al., 2018) to allow any effective separation between the two.

Cl atoms have more significant impact on the oxidation of some other VOCs. Tropospheric oxidation by Cl atoms in the model accounts for 20%, 14%, 10%, and 4% of the global losses of ethane (C_2H_6), propane (C_3H_8), higher alkanes, and methanol (CH_3OH).

Atmos. Chem. Phys. Discuss., https://doi.org/10.5194/acp-2018-1088
Manuscript under review for journal Atmos. Chem. Phys.
Discussion started: 19 October 2018

5.2 Impact on bromine and iodine chemistry

Bromine radicals ($BrO_x \equiv Br + BrO$) and iodine radicals ($IO_x \equiv I + IO$) affect global tropospheric chemistry by depleting ozone and OH (Parrella et al., 2012; Sherwen et al., 2016b). Br atoms are also thought to drive the oxidation of elemental mercury (Holmes et al., 2006). Chlorine chemistry increases IO_x mixing ratios by 16% due to reactions $HOI/INO_2/INO_3 + Cl^-$ (R10-R12), producing ICl which photolyzes rapidly to I atoms (Figure 1). The effect on bromine is more complicated. Bromine radicals originate from photolysis and oxidation of organobromines emitted by the ocean, as well as from SSA debromination (Yang et al., 2005). They are lost by conversion to HBr which is efficiently deposited. Parrella et al. (2012) pointed out that heterogeneous chemistry of HBr (dissolved as Br^-) is critical for recycling bromine radicals and explaining observed tropospheric BrO mixing ratios:

$$HOBr(aq) + Br^- + H^+ \rightarrow Br_2 + H_2O \quad \text{(R13)}$$

$$Br_2 + h\nu \rightarrow 2Br \quad \text{(R14)}$$

Chloride ions and dissolved SO_2 ($S(IV) \equiv HSO_3^- + SO_3^{2-}$) can however compete with Br^- for the available HOBr (aq) (Chen et al., 2017):

$$HOBr(aq) + Cl^- + H^+ \rightarrow BrCl + H_2O \quad \text{(R5)}$$

$$HOBr(aq) + HSO_3^-/SO_3^{2-} \rightarrow HBr + HSO_4^-/SO_4^{2-} \quad \text{(R15)}$$

Chen et al. (2017) pointed out that reaction (R15) effectively decreases BrO mixing ratios by producing HBr which is rapidly deposited instead of contributing to BrO_x cycling. They found in a GEOS-Chem simulation that global tropospheric BrO mixing ratios decreased by a factor of 2 as a result. Reaction (R5) may however have a compensating or opposite effect. It propagates the cycling of BrO_x if BrCl volatilizes:

$$BrCl + h\nu \rightarrow Br + Cl \quad \text{(R16)}$$

but it may also generate new BrO_x if BrCl reacts with Br^- in the aqueous phase to produce Br_2 (Wang et al., 1994):

$$BrCl(aq) + Br^- \rightleftarrows Br_2Cl^- \quad \text{(R17)}$$

$$Br_2Cl^- \rightleftarrows Br_2(aq) + Cl^- \quad \text{(R18)}$$

The sequence (R5) + (R17) + (R18) with Cl^- as a catalyst has the same stoichiometry as (R13) and thus contributes to HBr recycling in the same way. We find in the model that it is globally 30 times faster than (R13) and therefore much more effective at regenerating bromine radicals. The ensemble of reactions (R5, R13, R17, and R18) can be expressed stoichiometrically as:

$$HOBr(aq) + YBr^- + (1-Y)Cl^- + H^+ \rightarrow YBr_2 + (1-Y)BrCl + H_2O \quad \text{(R19)}$$

Atmos. Chem. Phys. Discuss., https://doi.org/10.5194/acp-2018-1088
Manuscript under review for journal Atmos. Chem. Phys.
Discussion started: 19 October 2018

where Y is the yield of Br_2 and 1-Y is the yield of BrCl. Y is calculated following the laboratory study of Fichert et al. (1999):

$$Y = 0.41\log_{10}([Br^-]/[Cl^-]) + 2.25 \quad \text{for } [Br^-]/[Cl^-] < 5 \times 10^{-4} \quad (2)$$

$$Y = 0.90 \quad \text{for } [Br^-]/[Cl^-] > 5 \times 10^{-4} \quad (3)$$

This mechanism was included in GEOS-Chem by Chen et al. (2017), who did not however have an explicit SSA Cl^- simulation (they instead assumed a fixed SSA $[Cl^-]$ = 0.5 M, and considered only dissolved HCl in cloud).

Chen et al. (2017) found in their GEOS-Chem simulation that the global tropospheric BrO burden was 8.7 Gg without the HOBr + S(IV) reaction (R15), and dropped to 3.6 Gg when the reaction was included. Previous GEOS-Chem model estimates of the global tropospheric BrO burden were 3.8 Gg (Parrella et al., 2012), 5.7 Gg (Schmidt et al., 2016), and 6.4 Gg (Sherwen et al., 2016b). Our simulation features many updates relative to Chen et al. (2017) including not only explicit SSA Cl^- but also explicit calculation of aerosol pH with ISORROPIA II for the rates of reactions in Table 2. By including explicit SSA Cl^-, the cloudwater $[Cl^-]$ in our model is much higher than that in Chen et al. (2017) and more comparable to measurements (~10^{-4} M in typical cloud; Straub et al., 2007). Thus we find in our standard simulation a global tropospheric BrO burden of 4.2 Gg, 17% higher than Chen et al. (2017).

Figure 9 shows the change of surface BrO mixing ratios due specifically to tropospheric chlorine chemistry, as obtained by difference with a sensitivity simulation including none of the Cl_y chemistry shown in Figure 2. The inclusion of chlorine chemistry increases the global tropospheric BrO burden by 85%. More than 80% of this change is caused by the HOBr + Cl^- reaction as discussed above. Other significant contributions include $ClNO_3$ + Br^- and $ClNO_2$ + Br^-. The largest BrO increases (1-2 ppt) are in surface air over the high northern latitudes oceans where SSA emissions are very high and acidic conditions promote HOBr + Cl^- chemistry.

5.3 Impact on tropospheric ozone and OH

Figure 9 shows the effects of chlorine chemistry on NO_x, OH, and ozone. .The global tropospheric burdens decrease by 5% for NO_x, 3% for OH, and 7% for ozone. The inter-hemispheric (N/S) ratio of trophospheric mean OH decreases from 1.14 to 1.12. Models tend to overestimate global mean tropospheric OH and its inter-hemispheric ratio relative to the constraint from methylchloroform (Naik et al., 2013, Voulgarakis et al., 2013), so the effect on OH is in the right direction.

The chlorine-induced decreases in Figure 9 are mainly through bromine chemistry initiated by chlorine (Section 5.2), and have spatial distributions characteristic of bromine chemistry with maxima at high latitudes as discussed by Schmidt et al. (2016). There are additional specific chlorine mechanisms including catalytic ozone loss through HOCl formation and photolysis:

Atmos. Chem. Phys. Discuss., https://doi.org/10.5194/acp-2018-1088
Manuscript under review for journal Atmos. Chem. Phys.
Discussion started: 19 October 2018

$$Cl + O_3 \rightarrow ClO + O_2 \quad \text{(R20)}$$

$$ClO + HO_2 \rightarrow HOCl + O_2 \quad \text{(R21)}$$

$$HOCl \xrightarrow{hv} Cl + OH \quad \text{(R22)}$$

Net: $O_3 + HO_2 \rightarrow OH + 2O_2$

and also loss of NO_x:

$$ClO + NO_2 + M \rightarrow ClNO_3 + M \quad \text{(R23)}$$

$$ClNO_3 + H_2O \rightarrow HOCl + HNO_3 \quad \text{(R24)}$$

But we find that these effects are very small compared to similar mechanisms involving bromine and iodine because the stability of HCl quenches Cl* radical cycling.

A particular situation arises over polluted continents due to $ClNO_2$ chemistry. Production of $ClNO_2$ at night from the N_2O_5 + Cl^- heterogeneous reaction, followed by photolysis in the morning to release Cl and NO_2, provides a source of radicals and ozone. This explains the increases of OH over North America and Europe in Figure 9. The effect is most important at high northern latitudes in winter due to the longer night. To isolate the impact on ozone we conducted a sensitivity simulation with no $ClNO_2$ production, setting $\varphi = 0$ for reaction (R3) in Table 2. The surface air ozone enhancement due to $ClNO_2$ chemistry is found to be the largest (~8 ppb) in European winter, due to the large supply of Cl^- from the North Atlantic combined with high NO_x emissions. Other polluted continents see ozone increases of 1-5 ppb in winter. The effect in summer is less than a ppb. These results are similar to previous regional modeling studies by Sarwar et al. (2014) and Sherwen et al. (2017).

6 Conclusions

We have added to the GEOS-Chem model a comprehensive and consistent representation of tropospheric chlorine chemistry. This includes in particular explicit accounting of the mobilization of sea salt aerosol (SSA) chloride (Cl^-), by acid displacement of HCl as well as by other heterogeneous processes. Cycling of inorganic gas-phase chlorine species (Cl_y) generated from SSA and other sources is simulated and coupled to the model aerosol-oxidant-bromine-iodine chemistry. With our work, GEOS-Chem now has a complete simulation of halogen (Cl+Br+I) chemistry in both the troposphere and stratosphere.

Emission of chlorine in the model is mainly as sea-salt aerosol (1780 Tg Cl a^{-1}). Other sources (combustion, organochlorines, stratospheric input) are also included but are small in comparison. Most of the sea-salt aerosol chloride is removed by deposition, but 3.6% is mobilized to inorganic gas-phase chlorine (Cl_y) through acid displacement to HCl (52 Tg a^{-1}) and

through other heterogeneous chemistry producing more reactive chlorine species (12 Tg a^{-1}). We define reactive chlorine (Cl*) as the ensemble of Cl_y species excluding HCl and including Cl, ClO, Cl_2, BrCl, HOCl, $ClNO_2$, $ClNO_3$, and other minor species. Oxidation of HCl by OH provides a Cl* source of 9.7 Tg a^{-1}, comparable to heterogeneous chemistry in particular HOBr + Cl^- (8.6 Tg a^{-1}). N_2O_5 + Cl^- (1.8 Tg a^{-1}) is also important in polluted environments. Cycling between Cl* species drives radical chlorine (Cl/ClO) chemistry but chain lengths are limited by fast conversion to HCl and subsequent deposition.

HCl mixing ratios in the model are highest over the oceans downwind of polluted continents due to effective acid displacement from sea-salt aerosol by HNO_3 and H_2SO_4. Mixing ratios are much lower over the Southern Ocean where the supply of acids is low. There is a secondary maximum of HCl in the upper troposphere due to stratospheric input. The dominant daytime Cl* species is generally HOCl while BrCl, Cl_2, and $ClNO_2$ dominate at night. $ClNO_3$ dominates in the upper troposphere due to stratospheric input. Chlorine atom concentrations are highest over Europe in winter due to $ClNO_2$ chemistry, and are otherwise high over the northern mid-latitudes oceans where the supply of acidity promotes Cl formation both through HCl and through other acid-catalyzed heterogeneous processes.

Comparison of model results to observations in marine surface air show that the model is able to reproduce the range and distributions of observed sea-salt aerosol chloride deficits, HCl mixing ratios, and Cl* mixing ratios. In particular, concurrent observations of HCl and HNO_3 in coastal/marine air worldwide show high correlation with the model including high HCl at northern mid-latitudes combined with depressed HNO_3. Consideration of acid displacement greatly improves model agreement with HNO_3 observations in marine air. The model can also successfully simulate observations of high $ClNO_2$ at night including in continental air. The chlorine in that case originates from sea-salt aerosol and can be transported far inland following uptake of volatilized HCl by sulfate-nitrate-ammonium (SNA) aerosol.

Comparisons of model results to aircraft campaign observations from WINTER (eastern US and offshore, Feb-Mar 2015), SEAC4RS (Southeast US, Aug-Sep 2013), and KORUS-AQ (Korean Peninsula, April-Jun 2016) show general consistency for HCl vertical profiles. Continental boundary layer HCl mixing ratios in these campaigns can be accounted for by the marine source transported inland. WINTER observations also include $ClNO_2$ and Cl_2, and HOCl. The observed $ClNO_2$ is mainly confined to the nighttime marine boundary layer and is consistent with the model. Observed Cl2 concentrations at night are much lower than the model, which has a large regional source from the $ClNO_2$ + Cl^- heterogeneous reaction. The rate coefficient for this reaction is from only one laboratory study. Observed Cl_2 concentrations in the daytime are often higher than at night, inconsistent with the model.

The model simulates a global mean Cl atom concentration of 620 cm^{-3} in the troposphere and 1200 cm^{-3} in the marine boundary layer (MBL), lower than previous global model studies that had excessive generation of Cl* but consistent with independent proxy constraints. We find that oxidation by Cl atoms accounts for only 1.0% of the global loss of atmospheric methane, and that the associated loss pattern is not sufficiently different from OH that it could be isolated in inversions of

atmospheric methane observations. Oxidation by Cl atoms has a larger effect on the global budgets of ethane (20%), propane (14%), and methanol (4%). Chlorine chemistry greatly stimulates the production of bromine radicals through the HOBr + Cl^- heterogeneous reaction, and increases global tropospheric BrO by 85% relative to a sensitivity simulation with no chlorine chemistry. Chlorine chemistry decreases the global burdens of tropospheric ozone and OH by 7% and 3% respectively, mainly through the induced bromine chemistry. An exception is winter conditions over polluted regions, where $ClNO_2$ chemistry increases ozone mixing ratios by up to 8 ppb.

Author contributions. XW, DJJ, and HL designed the study. XW developed the chlorine model code, performed the simulations and analyses. SDE, MPS, LZ, QC, BA, TS, and MJE contributed to the GEOS-Chem halogen model development. BHL, JDH, FDL, and JAT conducted and processed the measurement during WINTER campaign. GLH conducted and processed the measurement during SEAC^{4}RS and KORUS-AQ campaigns. XW and DJJ prepared the manuscript with contributions from all co-authors.

Data availability. The model code is available from the corresponding author upon request, and will be made available to the community through the standard GEOS-Chem (http://www.geos-chem.org) in the future. Data of WINTER campaign are available to the general public at https://www.eol.ucar.edu/field_projects/winter. Data of NASA SEAC^{4}RS AND KORUS-AQ missions and are available to the general public through the NASA data archive (https://www-air.larc.nasa.gov/cgi-bin/ArcView/seac4rs and https://www-air.larc.nasa.gov/cgi-bin/ArcView/korusaq).

Acknowledgments. This work was supported by the Atmospheric Chemistry Program of the US National Science Foundation and by the Joint Laboratory for Air Quality and Climate (JLAQC) between Harvard and the Nanjing University for Information Science and Technology (NUIST). QC and BA were supported by National Science Foundation (AGS 1343077). WINTER data are provided by NCAR/EOL under sponsorship of the National Science Foundation (https://www.eol.ucar.edu/field_projects/winter). SEAC^{4}RS and KORUS-AQ data are provided by NASA LaRC Airborne Science Data for Atmospheric Composition (https://www-air.larc.nasa.gov).

References

Abbatt, J. P. D., Lee, A. K. Y., and Thornton, J. A.: Quantifying trace gas uptake to tropospheric aerosol: recent advances and remaining challenges, Chem. Soc. Rev., 41, 6555–6581, doi:10.1039/c2cs35052a, 2012.

Alexander, B.: Sulfate formation in sea-salt aerosols: Constraints from oxygen isotopes, J. Geophys. Res., 110, D10307, doi:10.1029/2004JD005659, 2005.

Alexander, B., Allman, D. J., Amos, H. M., Fairlie, T. D., Dachs, J., Hegg, D. A., and Sletten, R. S.: Isotopic constraints on the formation pathways of sulfate aerosol in the marine boundary layer of the subtropical northeast Atlantic Ocean, J. Geophys. Res., 117, D06304, doi:10.1029/2011JD016773, 2012.

Allan, W., Lowe, D. C., and Cainey, J. M.: Active chlorine in the remote marine boundary layer: Modeling anomalous measurements of d13C in methane, Geophys. Res. Lett., 28, 3239–3242, 2011.

Ammann, M., Cox, R. A., Crowley, J. N., Jenkin, M. E., Mellouki, A., Rossi, M. J., Troe, J., and, Wallington, T. J.: Evaluated kinetic and photochemical data for atmospheric chemistry: Volume VI – heterogeneous reactions with liquid substrates, Atmos. Chem. Phys., 13, 8045–8228, doi:10.5194/acp-13-8045-2013, 2013.

Amos, H. M., D. J. Jacob, C. D. Holmes, J. A. Fisher, Q. Wang, R. M. Yantosca, E. S. Corbitt, E. Galarneau, A. P. Rutter, M. S. Gustin, A. Steffen, J. J. Schauer, J. A. Graydon, V. L. St. Louis, R. W. Talbot, E. S. Edgerton, Y. Zhang, and E. M. Sunderland, Gas-Particle Partitioning of Atmopsheric Hg(II) and Its Effect on Global Mercury Deposition, Atmos. Chem. Phys.,12,591-603, 2012.

Atkinson, R.: Gas-Phase Tropospheric Chemistry of Volatile Organic Compounds: 1. Alkanes and Alkenes, Journal of Physical and Chemical Reference Data, 26(2): 215-290, 1997.

ATom Science Team, Moffett Field, CA, NASA Ames Earth Science Project Office (ESPO), Accessed at doi: 10.5067/Aircraft/ATom/TraceGas_Aerosol_Global_Distribution, 2017.

Auzmendi-Murua, I., Castillo, A., and Bozzelli, J.: Mercury Oxidation via Chlorine, Bromine, and Iodine under Atmospheric Conditions: Thermochemistry and Kinetics, J. Phys. Chem. A, 118, 2959–2975, doi:10.1021/jp412654s, 2014.

Bannan, T. J., Booth, A. M., Bacak, A., Muller, J. B. A., Leather, K. E., Le Breton, M., Jones, B., Young, D., Coe, H., Allan, J., Visser, S., Slowik, J. G., Furger, M., Prévôt, A. S. H., Lee, J., Dunmore, R. E., Hopkins, J. R., Hamilton, J. F., Lewis, A. C., Whalley, L. K., Sharp, T., Stone, D., Heard, D. E., Fleming, Z. L., Leigh, R., Shallcross, D. E., and Percival, C. J.: The first UK measurements of nitryl chloride using a chemical ionization mass spectrometer in central London in the summer of 2012, and an investigation of the role of Cl atom oxidation, J. Geophys. Res.-Atmos., 120, 5638–5657, doi:10.1002/2014JD022629, 2015.

Bari, A., V. Ferraro, L. R. Wilson, D. Luttinger, and L. Husain (2003), Measurements of gaseous HONO, HNO_3,SO_2, HCl, NH3, particulate sulfate and PM2.5 in New York, NY, Atmos. Environ., 37(20), 2825–2835, doi:10.1016/S1352-2310(03)00199-7, 2003.

Beckwith, R. C., Wang, T. X., and Margerum, D. W.: Equilibrium and Kinetics of Bromine Hydrolysis, Inorg. Chem., 35, 995– 1000, 1996.

Behnke, W., C. George, V. Scheer, and C. Zetzsch (1997), Production and decay of ClNO2 from the reaction of gaseous N2O5 with NaCl solution: Bulk and aerosol experiments, J. Geophys. Res., 102(D3), 3795–3804, doi: 10.1029/96JD03057.

Bertram, T. H. and Thornton, J. A.: Toward a general parameterization of N2O5 reactivity on aqueous particles: the competing effects of particle liquid water, nitrate and chloride, Atmos. Chem. Phys., 9, 8351–8363, doi:10.5194/acp-9-8351-2009, 2009.

Chang, S. et al.: Sensitivity of urban ozone formation to chlorine emission estimates, Atmospheric Environment, 36(32), 4991-5003, 2002.

Chen, Q., J. A. Schmidt, V. Shah, L. Jaeglé, T. Sherwen, and B. Alexander: Sulfate production by reactive bromine: Implications for the global sulfur and reactive bromine budgets, Geophys. Res. Lett., 44, 7069–7078, doi:10.1002/2017GL073812, 2017.

Chen, Q., Sherwen, T., Evans, M., and Alexander, B.: DMS oxidation and sulfur aerosol formation in the marine troposphere: a focus on reactive halogen and multiphase chemistry, Atmos. Chem. Phys. Discuss., https://doi.org/10.5194/acp-2018-410, in review, 2018.

Crisp, T. A., B. M. Lerner, E. J. Williams, P. K. Quinn, T. S. Bates, and T. H. Bertram: Observations of gas phase hydrochloric acid in the polluted marine boundary layer, J. Geophys. Res. Atmos., 119, 6897–6915, doi:10.1002/2013JD020992, 2014.

Dahneke, B.: Simple Kinetic Theory of Brownian Diffusion in Vapors and Aerosols. In Theory of Dispersed Multiphase Flow, edited by R. E. Meyer. Academic Press, New York, pp. 97-133, 1983.

Dasgupta, P. K., S. W. Campbell, R. S. Al-Horr, S. M. R. Ullah, J. Z. Li, C. Amalfitano, and N. D. Poor: Conversion of sea salt aerosol to $NaNO_3$ and the production of HCl: Analysis of temporal behavior of aerosol chloride/nitrate and gaseous HCl/HNO_3 concentrations with AIM, Atmos. Environ., 41(20), 4242–4257, doi:10.1016/j.atmosenv.2006.09.054, 2007.

DeCarlo, P. F., Kimmel, J. R., Trimborn, A., Northway, M. J., Jayne, J. T., Aiken, A. C., Gonin, M., Fuhrer, K., Horvath, T., Docherty, K. S., Worsnop, D. R., and Jimenez, J. L.: Field-deployable, high-resolution, time-of-flight aerosol mass spectrometer, Anal. Chem., 78, 8281–8289, https://doi.org/10.1021/ac061249n, 2006.

Eastham, S. D., Weisenstein, D. K., and Barrett, S. R. H.: Development and evaluation of the unified tropospheric–stratospheric chemistry extension (UCX) for the global chemistry-transport model GEOS-Chem, Atmos. Environ., 89, 52–63, doi:10.1016/j.atmosenv.2014.02.001, 2014.

Faxon, C. B., Bean, J. K., and Ruiz, L. H.: Inland Concentrations of Cl_2 and $ClNO_2$ in Southeast Texas Suggest Chlorine Chemistry Significantly Contributes to Atmospheric Reactivity, Atmosphere, 6, 1487, doi:10.3390/atmos6101487, 2015.

Fickert, S., Adams, J. W., and Crowley, J. N.: Activation of Br_2 and BrCI via uptake of HOBr onto aqueous salt solutions, J. Geophys. Res., 104(D19): 23719-23727, 1999.

Finlayson-Pitts, B. J.: The Tropospheric Chemistry of Sea Salt: A Molecular-Level View of the Chemistry of NaCl and NaBr, Chem. Rev., 2003,103, 4801-4822.

Fountoukis, C. and Nenes, A.: ISORROPIA II: a computationally efficient thermodynamic equilibrium model for K^+–Ca^{2+}–Mg^{2+}–NH_4^+–Na^+–SO_4^{2-}–NO_3^-–Cl^-–H_2O aerosols, Atmos. Chem. Phys., 7, 4639-4659, https://doi.org/10.5194/acp-7-4639-2007, 2007.

Fridlind, A. M., and Jacobson, M. Z.: A study of gas-aerosol equilibrium and aerosol pH in the remote marine boundary layer duringthe first aerosol characterization experiment (ACE 1), J. Geophys. Res., 105(D13), 17,325–17,340, doi:10.1029/2000JD900209, 2000.

Giglio, L., Randerson, J. T., and van der Werf, G. R.: Analysis of daily, monthly, and annual burned area using the fourth generation global fire emissions database (GFED4) J. Geophys. Res.- Biogeo., 118, 317–328, 2013.

Graedel, T. E. and Keene, W. C.: Tropospheric budget of reactive chlorine, Global Biogeochemical Cycles, 9(1), 47-77, 1995.

Gromov, S., Brenninkmeijer, C. A. M., and Jöckel, P.: A very limited role of tropospheric chlorine as a sink of the greenhouse gas methane, Atmos. Chem. Phys., 18, 9831-9843, https://doi.org/10.5194/acp-18-9831-2018, 2018.

Guo, H., Sullivan, A. P., Campuzano-Jost, P., Schroder, J. C., Lopez-Hilfiker, F. D., Dibb, J. E., … Weber, R. J.: Fine particle pH and the partitioning of nitric acid during winter in the northeastern United States. Journal of Geophysical Research: Atmospheres, 121(17), 10355–10376, doi:10.1002/2016jd025311, 2016.

Heald, C. L., Collett Jr., J. L., Lee, T., Benedict, K. B., Schwandner, F. M., Li, Y., Clarisse, L., Hurtmans, D. R., Van Damme, M., Clerbaux, C., Coheur, P.-F., Philip, S., Martin, R. V., and Pye, H. O. T.: Atmospheric ammonia and particulate inorganic nitrogen over the United States, Atmos. Chem. Phys., 12, 10295–10312, doi:10.5194/acp-12-10295-2012, 2012.

Hoffmann, E. H., Tilgner, A., Schrödner, R., Bräuer, P., Wolke, R., and Herrmann, H.: An advanced modeling study on the impacts and atmospheric implications of multiphase dimethyl sulfide chemistry, P. Natl. Acad. Sci. USA, 113, 11776–11781, doi: 10.1073/pnas.1606320113, 2016.

Holmes, C. D., Jacob, D. J., and Yang, X.: Global lifetime of elemental mercury against oxidation by atomic bromine in the free troposphere , Geophys. Res. Lett. 33, L20808, doi:10.1029/2006GL027176， 2006.

Holmes, C. D., Jacob, D. J., Mason, R. P., and Jaffe, D. A.: Sources and deposition of reactive gaseous mercury in the marine atmosphere, Atmospheric Environment, 43, 2278-2285, 10.1016/j.atmosenv.2009.01.051, 2009.

Horowitz, H. M., Jacob, D. J., Zhang, Y., Dibble, T. S., Slemr, F., Amos, H. M., Schmidt, J. A., Corbitt, E. S., Marais, E. A., and Sunderland, E. M.: A new mechanism for atmospheric mercury redox chemistry: implications for the global mercury budget, Atmos. Chem. Phys., 17, 6353-6371, https://doi.org/10.5194/acp-17-6353-2017, 2017.

Haskins et al.: Inorganic chlorine budget and gas-particle partitioning in the winter low troposphere over the northeast United States, J. Geophys. Res., in review.

Hossaini, R., M. P. Chipperfield, A. Saiz-Lopez, R. Fernandez, S. Monks, W. Feng, P. Brauer, and R. von Glasow: A global model of tropospheric chlorine chemistry: Organic versus inorganic sources and impact on methane oxidation, J. Geophys. Res. Atmos., 121, 14,271–14,297, doi:10.1002/ 2016JD025756, 2016.

Impey, G. A., P. B. Shepson, D. R. Hastie, L. A. Barrie, and K. G. Anlauf: Measurements of photolyzable chlorine and bromine during the Polar Sunrise Experiment 1995, J. Geophys. Res., 102(D13), 16005–16010, doi: 10.1029/97JD00851, 1997.

Impey, G., Mihele, C., Anlauf, K. et al.: Measurements of Photolyzable Halogen Compounds and Bromine Radicals During the Polar Sunrise Experiment 1997, Journal of Atmospheric Chemistry, 34: 21. https://doi.org/10.1023/A:1006264912394, 1999.

Jacob, D. J., Waldman, J. M., Munger, J. W., and Hoffmann, M. R.: Chemical composition of fogwater collected along the California coast, Environ. Sci. Technol., 19, 730-736, 1985.

Jacob, D. J.: Heterogeneous chemistry and tropospheric ozone, Atmos. Environ., 34, 2131–2159, doi:10.1016/S1352-2310(99)00462-8, 2000.

Jaeglé, L., Quinn, P. K., Bates, T. S., Alexander, B., and Lin, J.-T.: Global distribution of sea salt aerosols: new constraints from in situ and remote sensing observations, Atmos. Chem. Phys., 11, 3137–3157, doi:10.5194/acp-11-3137-2011, 2011.

Kasibhatla, P., Sherwen, T., Evans, M. J., Carpenter, L. J., Reed, C., Alexander, B., Chen, Q., Sulprizio, M. P., Lee, J. D., Read, K. A., Bloss, W., Crilley, L. R., Keene, W. C., Pszenny, A. A. P., and Hodzic, A.: Global impact of nitrate photolysis in sea-salt aerosol on NO_x, OH, and O_3 in the marine boundary layer, Atmos. Chem. Phys., 18, 11185-11203, https://doi.org/10.5194/acp-18-11185-2018, 2018.

Keen, W. C. et al.: The geochemical cycling of reactive chlorine through the marine troposphere, Global Biogeochemical Cycles, 4(4), 407-430, 1990.

Keene, W. C., Stutz, J., Pszenny, A. A. P., Maben, J. R., Fischer, E., Smith, A. M., von Glasow, R., Pechtl, S., Sive, B. C., and Varner, R. K.: Inorganic chlorine and bromine in coastal New England air during summer, J. Geophys. Res., 112, D10S12, doi:10.1029/2006JD007689, 2007.

Keene, W. C., Long, M. S., Pszenny, A. A. P., Sander, R., Maben, J. R., Wall, A. J., O'Halloran, T. L., Kerkweg, A., Fischer, E. V., and Schrems, O.: Latitudinal variation in the multiphase chemical processing of inorganic halogens and related species over the eastern North and South Atlantic Oceans, Atmos. Chem. Phys., 9, 7361–7385, doi:10.5194/acp-9-7361-2009, 2009.

Kelly, J. T., Bhave, P. V., Nolte, C. G., Shankar, U., and Foley, K. M.: Simulating emission and chemical evolution of coarse sea-salt particles in the Community Multiscale Air Quality (CMAQ) model, Geosci. Model Dev., 3, 257-273, https://doi.org/10.5194/gmd-3-257-2010, 2010.

Kercher, J. P., T. P. Reidel, and J. A. Thornton: Chlorine activation by N_2O_5: Simulations, in situ detection of $ClNO_2$ and N_2O_5 by chemical ionization mass spectrometry, Atmos. Meas. Tech., 2, 193-204, 2009.

Kim, S., and Park, R. KORUS-AQ: An International Cooperative Air Quality Field Study in Korea, the KORUS-AQ white paper, 2014.

Kim, P. S., Jacob, D. J., Fisher, J. A., Travis, K., Yu, K., Zhu, L., Yantosca, R. M., Sulprizio, M. P., Jimenez, J. L., Campuzano-Jost, P., Froyd, K. D., Liao, J., Hair, J. W., Fenn, M. A., Butler, C. F., Wagner, N. L., Gordon, T. D., Welti, A., Wennberg, P. O., Crounse, J. D., St. Clair, J. M., Teng, A. P., Millet, D. B., Schwarz, J. P., Markovic, M. Z., and Perring, A. E.: Sources, seasonality, and trends of southeast US aerosol: an integrated analysis of surface, aircraft, and satellite observations with the GEOS-Chem chemical transport model, Atmos. Chem. Phys., 15, 10411-10433, https://doi.org/10.5194/acp-15-10411-2015, 2015.

Knipping, E. M. and Dabdub, D.: Modeling Cl_2 formation from aqueous NaCl particles: Evidence for interfacial reactions and importance of Cl_2 decomposition in alkaline solution, J. Geophys. Res., 107 (D18), 4360, doi:10.1029/2001JD000867, 2002.

Koepke, P., M. Hess, I. Schult, and E. P. Shettle, Global Aerosol Data Set, Report No. 243, Max-Planck-Institut fur Meteorologie, Hamburg, ISSN 0937-1060, 1997.

Kolesar, K. R. et al.: Increases in wintertime PM2.5 sodium and chloride linked to snowfall and road salt application, Atmospheric Environment, 177, 192-202, 2018.

Koo, B., Gaydos, T. M., and Pandis, S. N.: Evaluation of the equilibrium, dynamic, and hybrid aerosol modeling approaches, Aerosol Sci. Technol., 37(1), 53–64, 2003.

Lawler, M. J., Sander, R., Carpenter, L. J., Lee, J. D., von Glasow, R., Sommariva, R., and Saltzman, E. S.: HOCl and Cl_2 observations in marine air, Atmos. Chem. Phys., 11, 7617-7628, https://doi.org/10.5194/acp-11-7617-2011, 2011.

Lee, B. H. et al.: Airborne observations of reactive inorganic chlorine and bromine species in the exhaust of coal-fired power plants, J. Geophys. Res., doi: 10.1029/2018JD029284, 2018.

Lewis, E. R. and Schwartz, S. E.: Sea Salt Aerosol Production: Mechanisms, Methods, Measurements, and Models: A Critical Review, American Geophysical Union, Washington, DC, 2004.

Liao J. et al.: High levels of molecular chlorine in the Arctic atmosphere, Nature Geosci, 7, 91-94, 2014.

Liu, H., D.J. Jacob, I. Bey, and R.M. Yantosca, *Constraints from 210Pb and 7Be on wet deposition and transport in a global three-dimensional chemical tracer model driven by assimilated meteorological fields*, J. Geophys. Res., **106**, 12,109-12,128, 2001.

Liu, Q. and D. W. Margerum: Equilibrium and kinetics of bromine chloride hydrolysis, Environ. Sci. Tech., 35, 1127–1133., 2001.

Liu, X., et al.: Agricultural fires in the southeastern U.S. during SEAC4RS: Emissions of trace gases and particles and evolution of ozone, reactive nitrogen, and organic aerosol, J. Geophys. Res. Atmos., 121, 7383–7414, doi:10.1002/2016JD025040, 2016.

Liu, Y., Fan, Q., Chen, X., Zhao, J., Ling, Z., Hong, Y., Li, W., Chen, X., Wang, M., and Wei, X.: Modeling the impact of chlorine emissions from coal combustion and prescribed waste incineration on tropospheric ozone formation in China, Atmos. Chem. Phys., 18, 2709-2724, https://doi.org/10.5194/acp-18-2709-2018, 2018.

Lobert, J. M., W. C. Keene, J. A. Logan, and R. Yevich: Global chlorine emissions from biomass burning: Reactive chlorine emissions inventory, J. Geophys. Res., 104, 8373–8389, doi:10.1029/1998JD100077, 1999.

Long, M. S., Keene, W. C., Easter, R. C., Sander, R., Liu, X., Kerkweg, A., and Erickson, D.: Sensitivity of tropospheric chemical composition to halogen-radical chemistry using a fully coupled size-resolved multiphase chemistry–global climate system: halogen distributions, aerosol composition, and sensitivity of climate-relevant gases, Atmos. Chem. Phys., 14, 3397-3425, https://doi.org/10.5194/acp-14-3397-2014, 2014.

Lowe, D.C., et al., Shipboard determination of ^{13}C in atmospheric methane in the Pacific, J. Geophys. Res., 24-26,125-26,135, 1999.

Massucci, M., Clegg, S. L., and Brimblecombe, P.: Equilibrium Partial Pressures, Thermodynamic Properties of Aqueous and Solid Phases, and Cl_2 Production from Aqueous HCl and HNO_3 and Their Mixtures, J. Phys. Chem. A, 1999, 103(21), 4209-4226, doi: 10.1021/jp9847179, 1999.

Martin, R.V., D.J. Jacob, R.M. Yantosca, M. Chin, and P. Ginoux: Global and regional decreases in tropospheric oxidants from photochemical effects of aerosols, J. Geophys. Res., 108, 4097, doi:10.1029/2002JD002622, 2003.

McCulloch, A., M. L. Aucott, C. M. Benkovitz, T. E. Graedel, G. Kleiman, P. M. Midgley, and Y.-F. Li: Global emissions of hydrogen chloride and chloromethane from coal combustion, incineration and industrial activities: Reactive chlorine emissions inventory, J. Geophys. Res., 104, 8391–8403, doi:10.1029/1999JD900025, 1999.

McNaughton, C. S., L. Thornhill, A. D. Clarke, S. G. Howell, M. Pinkerton, B. Anderson, E. Winstead, C. Hudgins, H. Maring, J. E. Dibb, and E. Scheuer: Results from the DC-8 inlet characterization experiment (DICE): Airborne versus surface sampling of mineral dust and sea salt aerosols, Aerosol Science and Technology, 40, 136-159, 2007.

Meng, Z., and Seinfeld, J. H.: Time Scales to Achieve Atmospheric Gas-Aerosol Equilibrium for Volatile Species, Atmos. Environ. 30: 2889-2900, 1996.

Mielke, L. H., Furgeson, A., and Osthoff, H. D.: Observation of $ClNO_2$ in a Mid-Continental Urban Environment, Environ. Sci. Technol., 45, 8889–8896, doi:10.1021/es201955u, 2011.

Millet, D. B., Guenther, A., Siegel, D. A., Nelson, N. B., Singh, H. B., de Gouw, J. A., Warneke, C., Williams, J., Eerdekens, G., Sinha, V., Karl, T., Flocke, F., Apel, E., Riemer, D. D., Palmer, P. I., and Barkley, M.: Global atmospheric budget of acetaldehyde: 3-D model analysis and constraints from in-situ and satellite observations, Atmos. Chem. Phys., 10, 3405-3425, https://doi.org/10.5194/acp-10-3405-2010, 2010.

Murray, L. T., D. J. Jacob, J. A. Logan, R. C. Hudman, and W. J. Koshak, Optimized regional and interannual variability of lightning in a global chemical transport model constrained by LIS/OTD satellite data, J. Geophys. Res., 117, D20307, doi:10.1029/2012JD017934, 2012.

Naik, V., Voulgarakis, A., Fiore, A. M., Horowitz, L. W., Lamarque, J.-F., Lin, M., Prather, M. J., Young, P. J., Bergmann, D., Cameron-Smith, P. J., Cionni, I., Collins, W. J., Dalsøren, S. B., Doherty, R., Eyring, V., Faluvegi, G., Folberth, G. A., Josse, B., Lee, Y. H., MacKenzie, I. A., Nagashima, T., van Noije, T. P. C., Plummer, D. A., Righi, M., Rumbold, S. T., Skeie, R., Shindell, D. T., Stevenson, D. S., Strode, S., Sudo, K., Szopa, S., and Zeng, G.: Preindustrial to present-day changes in tropospheric hydroxyl radical and methane lifetime from the Atmospheric Chemistry and Climate Model Intercomparison Project (ACCMIP), Atmos. Chem. Phys., 13, 5277-5298, https://doi.org/10.5194/acp-13-5277-2013, 2013.

Ordóñez, C., Lamarque, J.-F., Tilmes, S., Kinnison, D. E., Atlas, E. L., Blake, D. R., Sousa Santos, G., Brasseur, G., and Saiz-Lopez, A.: Bromine and iodine chemistry in a global chemistry-climate model: description and evaluation of very short-lived oceanic sources, Atmos. Chem. Phys., 12, 1423–1447, doi:10.5194/acp-12-1423-2012, 2012.

Osthoff, H. D., Roberts, J. M., Ravishankara, A. R.,Williams, E. J., Lerner, B. M., Sommariva, R., Bates, T. M., Coffman, D., Quinn, P. K., Dibb, J. E., Stark, H., Burkholder, J. B., Talukdar, R. K., Meagher, J., Fehsenfeld, F. C., and Brown, S. S.: High levels of nitryl chloride in the polluted subtropical marine boundary layer, Nature Geosci., 1, 324–328, doi:10.1038/ngeo177, 2008.

Parrella, J. P., Jacob, D. J., Liang, Q., Zhang, Y., Mickley, L. J., Miller, B., Evans, M. J., Yang, X., Pyle, J. A., Theys, N., and Van Roozendael, M.: Tropospheric bromine chemistry: implications for present and pre-industrial ozone and mercury, Atmos. Chem. Phys., 12, 6723–6740, doi:10.5194/acp-12-6723-2012, 2012.

Pilinis, C., Capaldo, K. P., Nenes, A., and Pandis, S. N.: MADM-A New Multicomponent Aerosol Dynamics Model, Aerosol Science and Technology, 32:5, 482-502, DOI: 10.1080/027868200303597, 2000.

Phillips, G. J., Tang, M. J., Thieser, J., Brickwedde, B., Schuster, G., Bohn, B., Lelieveld, J., and Crowley, J. N.: Significant concentrations of nitryl chloride observed in rural continental Europe associated with the influence of sea salt chloride and anthropogenic emissions, Geophys. Res. Lett., 39, L10811, doi:10.1029/2012GL051912, 2012.

Platt, U., W. Allan, and D. Lowe: Hemispheric average Cl atom concentration from 13C/12C ratios in atmospheric methane, Atmos. Chem. Phys., 4, 2393–2399, doi:10.5194/acp-4-2393-2004, 2004.

Prather, M. J., Holmes, C. D., and Hsu, J.: Reactive greenhouse gas scenarios: Systematic exploration of uncertainties and the role of atmospheric chemistry, Geophysical Research Letters, 39, L09803, 10.1029/2012GL051440, 2012.

Pratte, P. and Rossi, M. J.: The heterogeneous kinetics of HOBr and HOCl on acidified sea salt and model aerosol at 40–90% relative humidity and ambient temperature, Phys. Chem. Chem. Phys., 8, 3988–4001, 2006.

Prinn, R. G., R.F. Weiss, P.B. Krummel, S. O'Doherty, P.J. Fraser, J. Muhle, S. Reimann, M.K. Vollmer, P.G. Simmonds, M. Maione, J. Arduini, C.R. Lunder, N. Schmidbauer, D. Young, H.J. Wang, J. Huang, M. Rigby, C.M. Harth, P.K. Salameh, T.G Spain, L.P. Steele, T. Arnold, J. Kim, O. Hermansen, N. Derek, B. Mitrevski, and R. Langenfelds (2016), The ALE / GAGE AGAGE Network, Carbon Dioxide Information Analysis Center (CDIAC), Oak Ridge National Laboratory (ORNL), U.S. Department of Energy (DOE).

Pszenny, A. A. P., W. C. Keene, D. J. Jacob, S. Fan, J. R. Maben, M. P. Zetwo, M. Springer-Young, and J. N. Galloway: Evidence of Inorganic Chlorine Gases Other Than Hydrogen Chloride in Marine Surface Air, Geophys. Res. Lett. 20(8): 699–702, doi:10.1029/93gl00047, 1993.

Pszenny, A. A. P., Moldanová, J., Keene,W. C., Sander, R., Maben, J. R., Martinez, M., Crutzen, P. J., Perner, D., and Prinn, R. G.: Halogen cycling and aerosol pH in the Hawaiian marine boundary layer, Atmos. Chem. Phys., 4, 147–168, doi:10.5194/acp-4-147-2004, 2004.

Riedel, T. P., Bertram, T. H., Crisp, T. A., Williams, E. J., Lerner, B. M., Vlasenko, A., Li, S.-M., Gilman, J., de Gouw, J., Bon, D. M., Wagner, N. L., Brown, S. S., and Thornton, J. A.: Nitryl Chloride and Molecular Chlorine in the Coastal Marine Boundary Layer, Environ. Sci. Technol., 46, 10463–10470, doi:10.1021/es204632r, 2012.

Roberts, T. J., Braban, C. F., Martin, R. S., Oppenheimer, C., Adams, J. W., Cox, R. A., Jones, R. L., and Griffiths, P. T.: Modelling reactive halogen formation and ozone depletion in volcanic plumes, Chem. Geol., 263, 151–163, 2009.

Saiz-Lopez, A., and von Glasow, R.: Reactive halogen chemistry in the troposphere, Chem. Soc. Rev., 2012,41, 6448-6472.

Sander, R., A. A. P. Pszenny, W. C. Keene, E. Crete, B. Deegan, M. S. Long, J. R. Maben, and A. H. Young: Gas phase acid, ammonia and aerosol ionic and trace element concentrations at Cape Verde during the Reactive Halogens in the Marine Boundary Layer (RHaMBLe) 2007 intensive sampling period, Earth Syst. Sci. Data, 5(2), 385–392, doi:10.5194/essd-5-385-2013, 2013.

Sander, R.: Compilation of Henry's law constants (version 4.0) for water as solvent, Atmos. Chem. Phys., 15, 4399-4981, https://doi.org/10.5194/acp-15-4399-2015, 2015.

Sanhueza, E., and A. Garaboto: Gaseous HCl at a remote tropical continental site, Tellus B, 54(4), 412–415, doi:10.1034/j.1600-0889.2002.251371.x, 2002.

Sarwar, G., Simon, H., Xing, J., and Mathur, R.: Importance of tropospheric $ClNO_2$ chemistry across the Northern Hemisphere, Geophys. Res. Lett., 41, 4050-4058, doi:10.1002/2014GL059962, 2014.

Schmidt, J. A., Jacob, D. J., Horowitz, H. M., Hu, L., Sherwen, T., Evans, M. J., Liang, Q., Suleiman, R. M., Oram, D. E., Breton, M. L., Percival, C. J.,Wang, S., Dix, B., and Volkamer, R.: Modeling the observed tropospheric BrO background: Importance of multiphase chemistry and implications for ozone, OH, and mercury, J. Geophys. Res.-Atmos., doi:10.1002/2015JD024229, 2016.

Simmonds, P. G. et al.: Global trends, seasonal cycles, and European emissions of dichloromethane, trichloroethene, and tetrachloroethene from the AGAGE observations at Mace Head, Ireland, and Cape Grim, Tasmania, J. Geophys. Res., 111, D18304, doi:10.1029/2006JD007082, 2006

Singh, H.B., and Kasting, J. F.: Chlorine-hydrocarbon photochemistry in the marine troposphere and lower stratosphere, J. Atmos. Chem., 7(3): 261-285, doi: 10.1007/BF00130933, 1988.

Simpson, W. R., Brown, S. S., Saiz-Lopez, A., Thornton, J. A., and von Glasow, R.: Tropospheric Halogen Chemistry: Sources, Cycling, and Impacts, Chemical Reviews, 2015, 115(10), 4035-4062, DOI: 10.1021/cr5006638.

Singh, H. B., Gregory, G. L., Anderson, B., Browell, E., Sachse, G. W., Davis, D. D., Crawford, J., Bradshaw, J. D., Talbot, R., Blake, D. R., Thornton, D., Newell, R., and Merrill, J.: Low ozone in the marine boundary layer of the tropical Pacific Ocean: Photochemical loss, chlorine atoms, and entrainment, J. Geophys. Res., 101, 1907–1917, 1996.

Sherwen, T., Evans, M. J., Carpenter, L. J., Andrews, S. J., Lidster, R. T., Dix, B., Koenig, T. K., Sinreich, R., Ortega, I., Volkamer, R., Saiz-Lopez, A., Prados-Roman, C., Mahajan, A. S., and Ordóñez, C.: Iodine's impact on tropospheric oxidants: a global model study in GEOS-Chem, Atmos. Chem. Phys., 16, 1161–1186, doi:10.5194/acp-16-1161-2016, 2016a.

Sherwen, T., Schmidt, J. A., Evans, M. J., Carpenter, L. J., Großmann, K., Eastham, S. D., Jacob, D. J., Dix, B., Koenig, T. K., Sinreich, R., Ortega, I., Volkamer, R., Saiz-Lopez, A., Prados-Roman, C., Mahajan, A. S., and Ordóñez, C.: Global impacts of tropospheric halogens (Cl, Br, I) on oxidants and composition in GEOS-Chem, Atmos. Chem. Phys., 16, 12239-12271, https://doi.org/10.5194/acp-16-12239-2016, 2016b.

Sherwen, T. et al.: Effects of halogens on European air-quality, Faraday Discuss., 200, 75, 2017.

Straub, D. J., Lee, T, and Collete Jr., J. L.: Chemical composition of marine stratocumulus clouds over the eastern Pacific Ocean, J. Geophys. Res., 112, D04307, doi:10.1029/2006JD007439, 2007.

Thornton, J. A., Kercher, J. P., Riedel, T. P., Wagner, N. L., Cozic, J., Holloway, J. S., Dubé,W. P.,Wolfe, G. M., Quinn, P. K., Middlebrook, A. M., Alexander, B., and Brown, S. S.: A large atomic chlorine source inferred from mid-continental reactive nitrogen chemistry, Nature, 464, 271–274, doi:10.1038/nature08905, 2010.

Toon, O. B., Maring, H., Dibb, J., Ferrare, R., Jacob, D. J., Jensen, E. J., Luo, Z. J., Mace, G. G., Pan, L. L., Pfister, L., Rosenlof, K. H., Redemann, J., Reid, J. S., Singh, H. B., Yokelson, R., Chen, G., Jucks, K. W., and Pszenny, A.: Planning, implementation, and scientific goals of the Studies of Em issions and Atmospheric Composition, Clouds and Climate Coupling by Regional Surveys (SEAC4RS) field mission, J. Geophys. Res.-Atmos., 121, 4967– 5009, https://doi.org/10.1002/2015JD024297, 2016.

US EPA: 2014 National Emissions Inventory, version 2 Technical Support Document, Office of Air Quality Planning and Standards, Research Triangle Park, NC, available at: https://www.epa.gov/air-emissions-inventories/2014-national-emissions-inventory-nei-data (last access: 28 August 2018), 2018.

van der Werf, G. R., Randerson, J. T., Giglio, L., Collatz, G. J., Mu, M., Kasibhatla, P. S., Morton, D. C., DeFries, R. S., Jin, Y., and van Leeuwen, T. T.: Global fire emissions and the contribution of deforestation, savanna, forest, agricultural, and peat fires (1997–2009), Atmos. Chem. Phys., 10, 11707–11735, https://doi.org/10.5194/acp-10-11707-2010, 2010.

Voulgarakis, A., Naik, V., Lamarque, J. F., Shindell, D. T., Young, P. J., Prather, M. J., Wild, O., Field, R. D., Bergmann, D., Cameron-Smith, P., Cionni, I., Collins, W. J., Dalsøren, S. B., Doherty, R. M., Eyring, V., Faluvegi, G., Folberth, G. A., Horowitz, L. W., Josse, B., MacKenzie, I. A., Nagashima, T., Plummer, D. A., Righi, M., Rumbold, S. T., Stevenson, D. S.,

Strode, S. A., Sudo, K., Szopa, S., and Zeng, G.: Analysis of present day and future OH and methane lifetime in the ACCMIP simulations, Atmos. Chem. Phys., 13, 2563-2587, 10.5194/acp-13-2563-2013, 2013.

Walker, J. M., Philip, S., Martin, R. V., and Seinfeld, J. H.: Simulation of nitrate, sulfate, and ammonium aerosols over the United States, Atmos. Chem. Phys., 12, 11213-11227, https://doi.org/10.5194/acp-12-11213-2012, 2012.

Wang, T., et al.: Observations of nitryl chloride and modeling its source and effect on ozone in the planetary boundary layer of southern China, J. Geophys. Res. Atmos., 121, 2476–2489, doi:10.1002/2015JD024556, 2016.

World Meteorological Organization (WMO), Scientific Assessment of Ozone Depletion: 2014, World Meteorological Organization, Global Ozone Research and Monitoring Project—Report No. 55, 416 pp., Geneva, Switzerland, 2014.

Yang, X., Cox, R. A., Warwick, N. J., Pyle, J. A., Carver, G. D., O'Connor, F. M., and Savage, N. H.: Tropospheric bromine chemistry and its impacts on ozone: A model study, J. Geophys. Res., 110, D23311, doi:10.1029/2005JD006244, 2005.

Zhang, Y., Jacob, D. J., Maasakkers, J. D., Sulprizio, M. P., Sheng, J.-X., Gautam, R., and Worden, J.: Monitoring Global Tropospheric OH Concentrations using Satellite Observations of Atmospheric Methane, Atmos. Chem. Phys. Discuss., https://doi.org/10.5194/acp-2018-467, in review, 2018.

Zhu et al.: Effect of sea-salt aerosol on tropospheric bromine chemistry, in prep, 2018.

Atmos. Chem. Phys. Discuss., https://doi.org/10.5194/acp-2018-1088
Manuscript under review for journal Atmos. Chem. Phys.
Discussion started: 19 October 2018

Atmospheric Chemistry and Physics Discussions

Table 1: Global sources and sinks of gas-phase inorganic (Cl_y) and reactive (Cl*) tropospheric chlorine [a].

	Cl_y (Gg Cl a^{-1})	Cl* (Gg Cl a^{-1})
Source	75200	25000
Sea Salt	63900	11900
Acid displacement [b]	52000	-
HOBr + Cl^-	8590	8590
N_2O_5 + Cl^-	1810	1810
HOI, $IONO_x$ [c] + Cl^-	641	641
$ClNO_2$ + Cl^-	327	327
OH + Cl^-	403	403
$ClNO_3$ + Cl^-	64	64
HOCl + Cl^-	61	61
HCl + OH	-	9720
Organochlorines	3320	3300
CH_3Cl + OH [d]	2200	2180
CH_2Cl_2 +OH	780	780
$CHCl_3$ + OH	298	298
CH_2ICl + OH	46	46
Stratosphere [e]	380	64
Anthropogenic HCl [f]	(6660)	-
Open fires	7640	-
Sinks	75200	25000
Deposition	71400	346
Dry	35200	170
Wet	36200	176
Uptake by alkaline SSA	3800	-
Conversion to HCl [g]	-	24600
Tropospheric mass (Gg)	316	12
Lifetime (hours)	37	3.8

[a] Annual totals for 2016 computed from GEOS-Chem. Gas-phase inorganic chlorine is defined as $Cl_y \equiv Cl + 2\times Cl_2 + 2\times Cl_2O_2 + ClNO_2 + ClNO_3 + ClO + ClOO + OClO + BrCl + ICl + HOCl + HCl$. Reactive chlorine is defined as $Cl^* \equiv Cl_y - HCl$. Thus the source of HCl can be inferred from the Table entries as $Cl_y - Cl^*$. The definition of Cl_y excludes aerosol Cl^-, which has a very large sea salt source of 1780 Tg Cl a^{-1} but is mainly removed by deposition, HCl is the dominant component of Cl_y but is also mostly removed by deposition. Reactive chlorine Cl* is the chemical family principally involved in radical cycling.

[b] Net production minus loss of HCl from acid aerosol displacement by HNO_3 and H_2SO_4 computed as thermodynamic equilibrium.

[d] The source from CH3Cl + Cl is not shown since it contributes < 1%. Same for other organochlorines.

[c] $IONO_x \equiv IONO + IONO_2$

[e] Net stratospheric input to the troposphere.

[f] Coal combustion, waste incineration, and industrial activities. These emissions are only included in a sensitivity simulation (see Section 2.2 and 4.2 for details) and are therefore listed here in parentheses.

[g] From reactions of Cl atoms (see Figure 1).

Atmos. Chem. Phys. Discuss., https://doi.org/10.5194/acp-2018-1088
Manuscript under review for journal Atmos. Chem. Phys.
Discussion started: 19 October 2018

Atmospheric Chemistry and Physics Discussions

Table 2: Heterogeneous reactions of Cl^- and reactive uptake coefficients (γ) [a].

	Reaction	Reactive uptake coefficient (γ)	Footnote
R3	$N_2O_5 + \varphi Cl^- + (1-\varphi)H_2O \rightarrow \varphi ClNO_2 + (2-\varphi)NO_3^- + 2(1-\varphi)H^+$	$\gamma = Bk'_{2f}\left(1 - \frac{1}{\left(\frac{k_3[H_2O]}{k_{2b}[NO_3^-]}\right) + 1 + \left(\frac{k_4[Cl^-]}{k_{2b}[NO_3^-]}\right)}\right)$ $k'_{2f} = \beta\left(1 - e^{-\delta[H_2O]}\right)$; $\varphi = \left(\frac{k_2[H_2O]}{k_3[Cl^-]} + 1\right)^{-1}$ $B = 3.2 \times 10^{-8} s$; $k_3/k_2 = 450$ $\beta = 1.15 \times 10^6 s^{-1}$; $\delta = 0.13 M^{-1}$ $k_3/k_{2b} = 0.06$; $k_4/k_{2b} = 29$	b
R4	$OH + Cl^- \rightarrow 0.5Cl_2 + OH^-$	$\gamma = 0.04[Cl^-]$	c
R5	$HOBr + Cl^- + H^+ \rightarrow BrCl + H_2O$	$\gamma = \left(\frac{1}{\Gamma_b} + \frac{1}{\alpha_b}\right)^{-1}$ $\Gamma_b = 4H_{HOBr}RTI_r k_b[Cl^-][H^+]f(r, I_r)/c$ $I_r = \sqrt{D_l/(k_b[Cl^-][H^+])}$; $\alpha_b = 0.6$ $k_b = 2.3 \times 10^{10} M^{-2}s^{-1}$; $D_l = 1.4 \times 10^{-5} cm^2 s^{-1}$	d
R6	$ClNO_3 + Cl^- \rightarrow Cl_2 + NO_3^-$	$\gamma = 0.0244$	e
R7	$ClNO_2 + Cl^- \rightarrow NO_2^- + Cl_2$	$\gamma = \left(\frac{1}{\Gamma_b} + \frac{1}{\alpha_b}\right)^{-1}$ (pH < 2), $\gamma = 0$ (pH > 2) $\Gamma_b = 4H_{ClNO_2}RTI_r k^{II}[Cl^-]f(r, I_r)/c$ $I_r = \sqrt{D_l/(k^{II}[Cl^-])}$; $\alpha_b = 0.01$ $k^{II} = 10^7 M^{-2}s^{-1}$; $D_l = 1 \times 10^{-5} cm^2 s^{-1}$	
R8	$HOCl + Cl^- + H^+ \rightarrow Cl_2 + H_2O$	$\gamma = \min\left(\left(\frac{1}{\Gamma_b} + \frac{1}{\alpha_b}\right)^{-1}, 2 \times 10^{-4}\right)$ $\Gamma_b = 4H_{HOCl}RTI_r k_t[Cl^-][H^+]f(r, I_r)/c$ $I_r = \sqrt{D_l/(k_t[Cl^-][H^+])}$; $\alpha_b = 0.8$ $k_t = 1.5 \times 10^4 M^{-2}s^{-1}$; $D_l = 2 \times 10^{-5} cm^2 s^{-1}$	
R9	$NO_3 + Cl^- \rightarrow NO_3^- + Cl^-$	$\gamma = \left(\frac{1}{\Gamma_b} + \frac{1}{\alpha_b}\right)^{-1}$ $\Gamma_b = 4H_{NO_3}RTI_r k'[Cl^-]f(r, I_r)/c$ $I_r = \sqrt{D_l/(k'[Cl^-])}$; $\alpha_b = 0.013$ $k' = 2.76 \times 10^6 M^{-2}s^{-1}$; $D_l = 1 \times 10^{-5} cm^2 s^{-1}$	
R10	$IONO_2 + Cl^- \rightarrow ICl + NO_3^-$	$\gamma = 8.5 \times 10^{-3}$	f
R11	$IONO + Cl^- \rightarrow ICl + NO_2^-$	$\gamma = 0.017$	f
R12	$HOI + Cl^- \rightarrow ICl + OH^-$	$\gamma = 8.5 \times 10^{-3}$	f

[a] Formulations for the reactive uptake coefficient γ are from IUPAC (Ammann et al., 2013) unless stated otherwise in the footnote column. Brackets denote aqueous-phase concentrations in unit of M (moles per liter of water). R is the ideal gas constant. c is the average gas-phase thermal velocity for the reactant with Cl^-. The reactive uptake coefficient is used to calculate the reaction rate following equation (1). $f(r, I_r) = \coth(r/I_r) - (I_r/r)$ is a spherical correction to mass transfer where I_r is a reacto-diffusive length scale and r is the radius of the aerosol particle or cloud droplet.

[b] Bertram and Thornton (2009); Roberts et al. (2009).

[c] Knipping and Dabdub (2002)

[d] k_b is based on Liu and Margerum (2001). R5 competes with the heterogeneous reactions $HOBr+Br^-$ and HOBr+S(IV) as given by Chen et al. (2017).

[e] Assumes that Cl^- is present in excess so that γ does not depend on $[Cl^-]$. However, R6 competes with the heterogeneous reaction $ClNO_3+Br^-$ as given by Schmidt et al. (2016), with the branching ratio determined by the relative rates.

[f] These reactions are based on Sherwen et al. (2016a) and only take place in SSA.

Atmos. Chem. Phys. Discuss., https://doi.org/10.5194/acp-2018-1088
Manuscript under review for journal Atmos. Chem. Phys.
Discussion started: 19 October 2018

Table 3: Chloride deficits in sea salt aerosol.[a]

Location	Modeled Cl^- deficit (%)	Measured Cl^- deficit (%)
North Carolina coast	+40	-1 to +90
Townsville coast, Australia	+23	+33
California coast	+21	+2 to +75
Greenland Sea	+18	+6 to +22
North Atlantic Ocean	+14	-24 to +54
Equatorial Atlantic	+12	+11 to +64
Puerto Rico coast	+9	+7 to +25
Pacific Ocean	+6	-22 ~ +40
Cape Grim, Australia	+4	-50~+15

[a] Deficits relative to seawater composition. Observations compiled by Graedel and Keene (1995) are reported there as ranges for individual regions and months, with the ranges likely reflecting measurement uncertainty rather than physical variability. Model values are means for the regions and months of observations.

Table 4: Surface air mixing ratios of reactive (Cl*)[a]

Location	Modeled Cl^* (ppt)	Measured mean Cl^* (ppt)	Reference
Atlantic cruise near Europe	43	27[b]	Keene et al. (2009)
Appledore Island (US east coast)	17	< 20	Keene et al. (2007)
Atlantic cruise near North Africa	5	< 24	Keene et al. (2009)
Southern Ocean cruise	4	< 24	Keene et al. (2009)
Hawaii	4	6	Pszenny et al. (2004)
Tropical Atlantic cruise	2	< 24	Keene et al. (2009)
Alert (Canada)	0.2	< 14	Impey et al. (1999)

[a] Reactive chlorine Cl* is the ensemble of gas-phase inorganic chlorine species excluding HCl. Measurements are 24- hour averages. Model values are monthly means in 2016 taken for the same month and location.
[b] Median value

Atmos. Chem. Phys. Discuss., https://doi.org/10.5194/acp-2018-1088
Manuscript under review for journal Atmos. Chem. Phys.
Discussion started: 19 October 2018

Atmospheric Chemistry and Physics Discussions

Table 5: Comparison of modeled maximum $ClNO_2$ mixing ratios to surface observations [a]

Location	Date	Observed (ppt)	Simulated (ppt)	References
London, UK	July-Aug 2012	730	510	Bannan et al. (2015)
Calgary, Canada	Apr 2010	240	130	Mielke et al. (2011)
Frankfurt, Germany	Aug-Sep 2011	850	400	Phillips et al. (2012)
Long Island Sound	Mar 2008	200	210	Kercher et al. (2009)
Boulder, Colorado	Feb 2009	440	130	Thornton et al. (2010)
Pasadena, California	May-Jun 2010	3500	360	Mielke et al. (2013)
Offshore of Los Angeles, California	May-Jun 2010	1800	500	Riedel et al. (2012)
Houston, Texas	Sep 2013	140	18	Faxon et al. (2015)
Hong Kong, China	Nov-Dec, 2013	4700	410	Wang et al. (2016)

[a] Observed and modeled values are maxima for the reporting period. Model maxima are based on hourly values sampled at the same location and time period as the observations.

Atmos. Chem. Phys. Discuss., https://doi.org/10.5194/acp-2018-1088
Manuscript under review for journal Atmos. Chem. Phys.
Discussion started: 19 October 2018

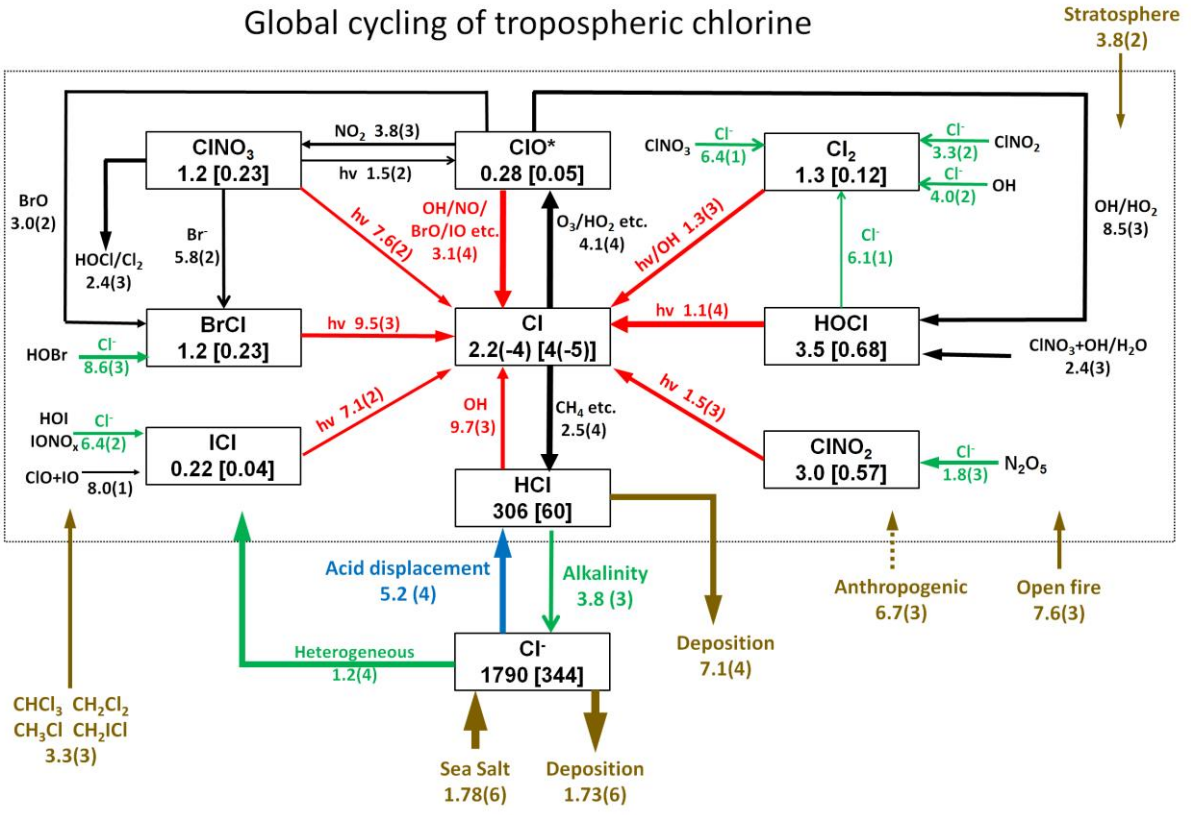

Figure 1: Global budget and cycling of tropospheric inorganic chlorine (Cl_y) in GEOS-Chem. The figure shows global annual mean rates (Gg Cl a^{-1}), masses (Gg), and mixing ratios (ppt, in brackets) for simulation year 2016. Read 2.5(4) as 2.5×10^4. ClO* stands for ClO + OClO + ClO_2 + $2Cl_2O_2$; 84% is present as ClO. Reactions producing Cl atoms and related to Cl^- heterogeneous chemistry are shown in red and green, respectively. The dotted box indicates the Cl_y family, and arrows into and out of that box represent general sources and sinks of Cl_y. Reactions with rate < 100 Gg Cl a^{-1} are not shown. Anthropogenic emissions of HCl as indicated by a dashed line are only included in a sensitivity simulation (see Section 2.2 and 4.2 for details).

Atmos. Chem. Phys. Discuss., https://doi.org/10.5194/acp-2018-1088
Manuscript under review for journal Atmos. Chem. Phys.
Discussion started: 19 October 2018

Atmospheric Chemistry and Physics Discussions

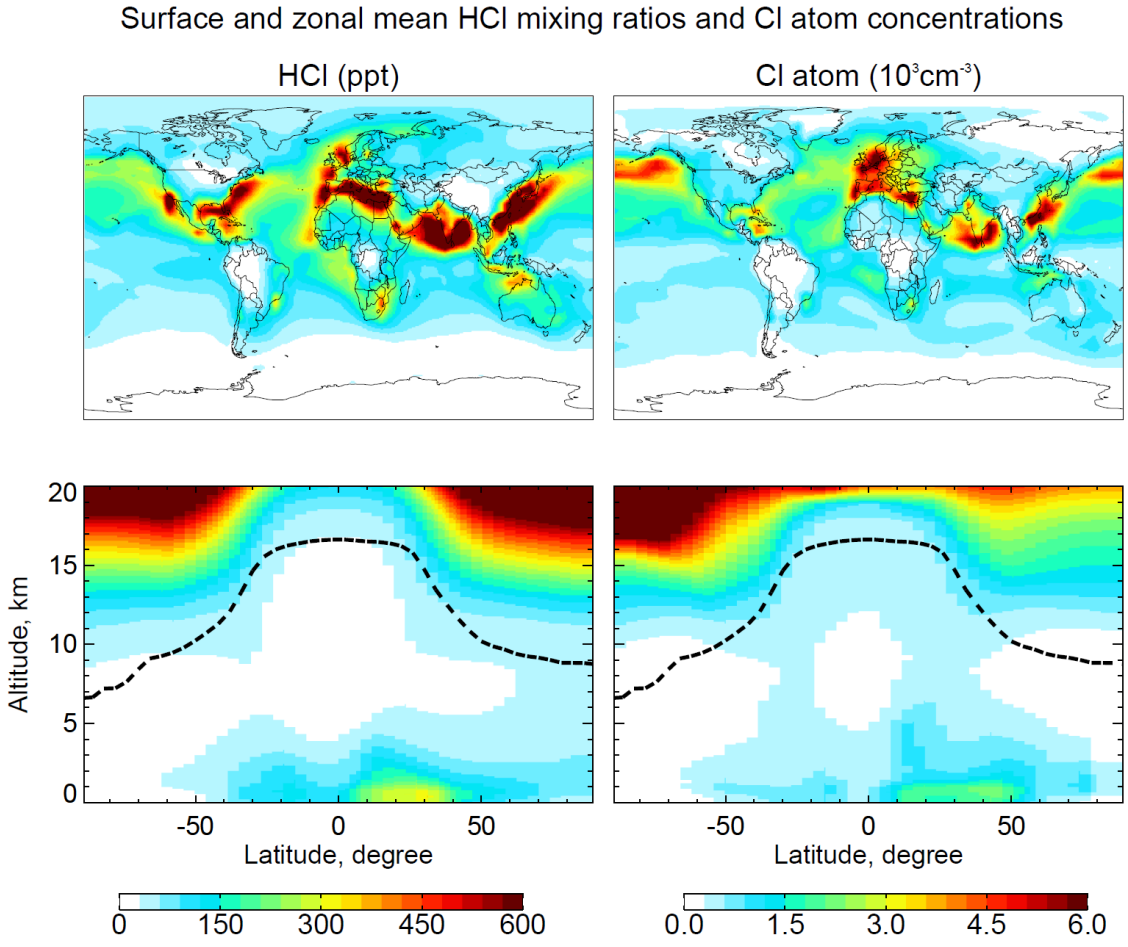

Figure 2: Global distributions of annual mean HCl mixing ratios and Cl atom concentrations in GEOS-Chem. The top panels show surface air mixing ratios/concentrations. The bottom panels show zonal mean mixing ratios/concentrations as a function of latitude and altitude. Dashed lines indicate the tropopause.

5

Atmos. Chem. Phys. Discuss., https://doi.org/10.5194/acp-2018-1088
Manuscript under review for journal Atmos. Chem. Phys.
Discussion started: 19 October 2018

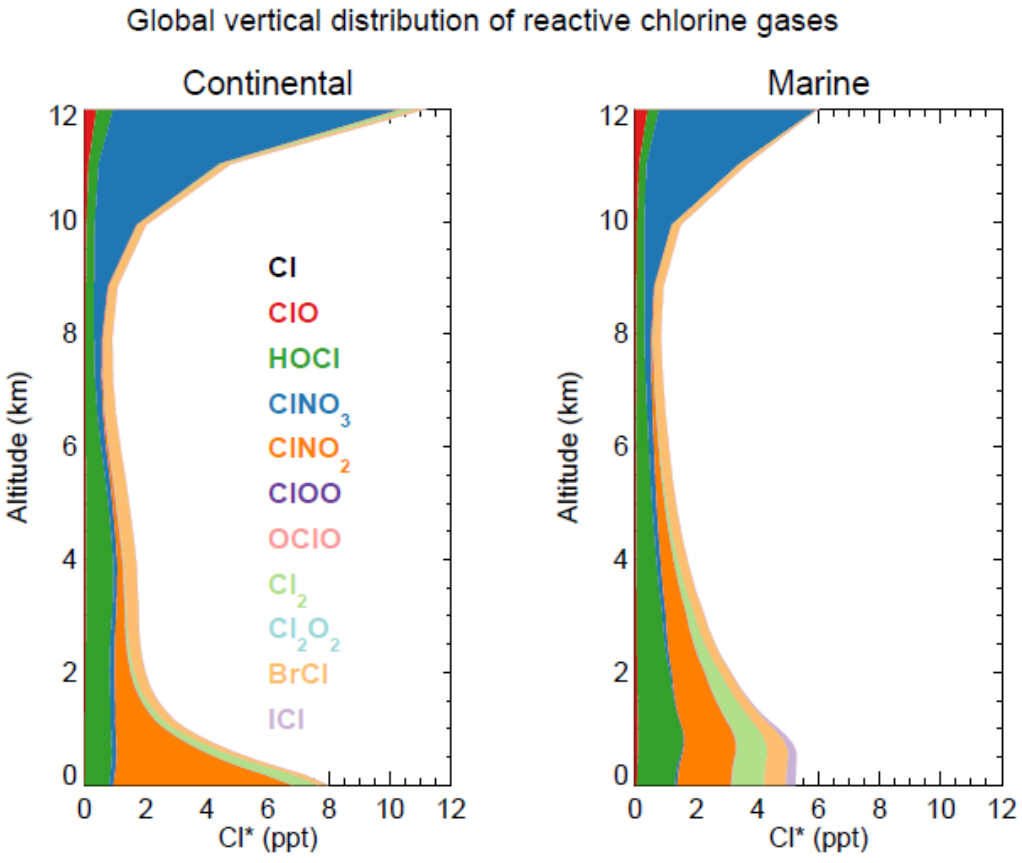

Figure 3: Global annual mean vertical distributions of reactive chlorine species (Cl*) in GEOS-Chem for continental and marine air. Stratospheric conditions are excluded.

Atmos. Chem. Phys. Discuss., https://doi.org/10.5194/acp-2018-1088
Manuscript under review for journal Atmos. Chem. Phys.
Discussion started: 19 October 2018

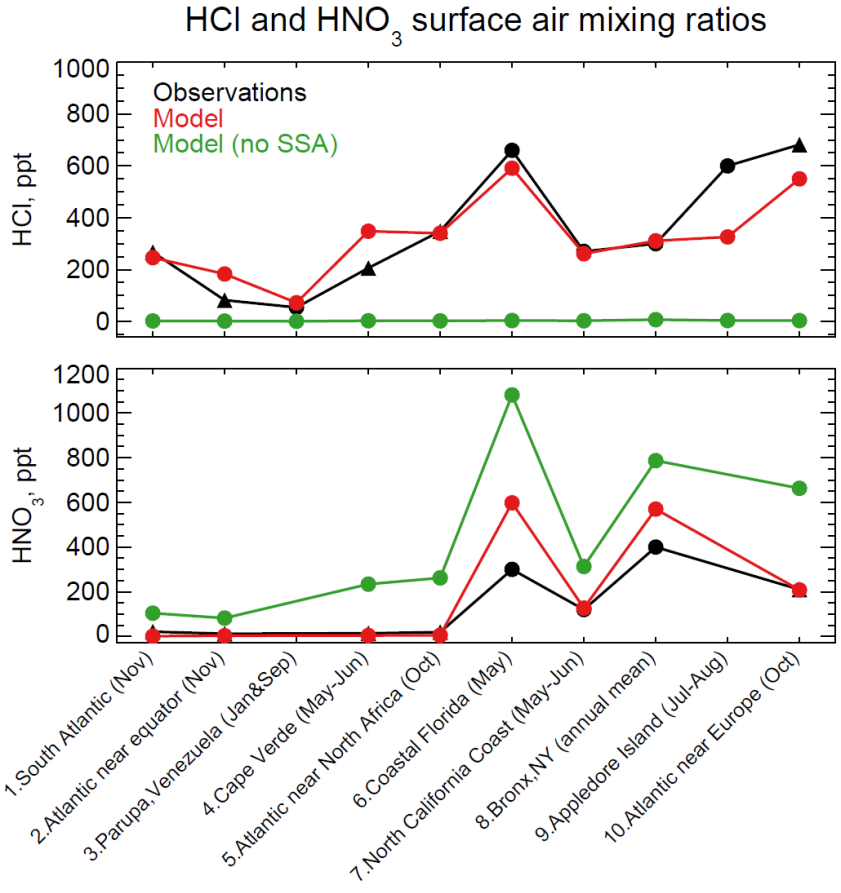

Figure 4: HCl and HNO_3 surface air mixing ratios at coastal/island sites and from ocean cruises. Observations are means (black circles) or medians (black triangles) depending availability. Model values are monthly means for the sampling locations. Also shown are results from a sensitivity simulation with no mobilization of Cl^- from sea salt aerosol (SSA). The measurements are arranged from south to north (left to right) and the lines illustrate the latitudinal gradients and correlations for model and observations. References: (1, 2, 5, 10) Keene et al. (2009); (3) Sanhueza et al. (2002); (4) Sander et al. (2013); (6) Dasgupta et al. (2007); (7) Crisp et al. (2014); (8) Bari et al. (2003); (9) Keene et al. (2007).

Atmos. Chem. Phys. Discuss., https://doi.org/10.5194/acp-2018-1088
Manuscript under review for journal Atmos. Chem. Phys.
Discussion started: 19 October 2018

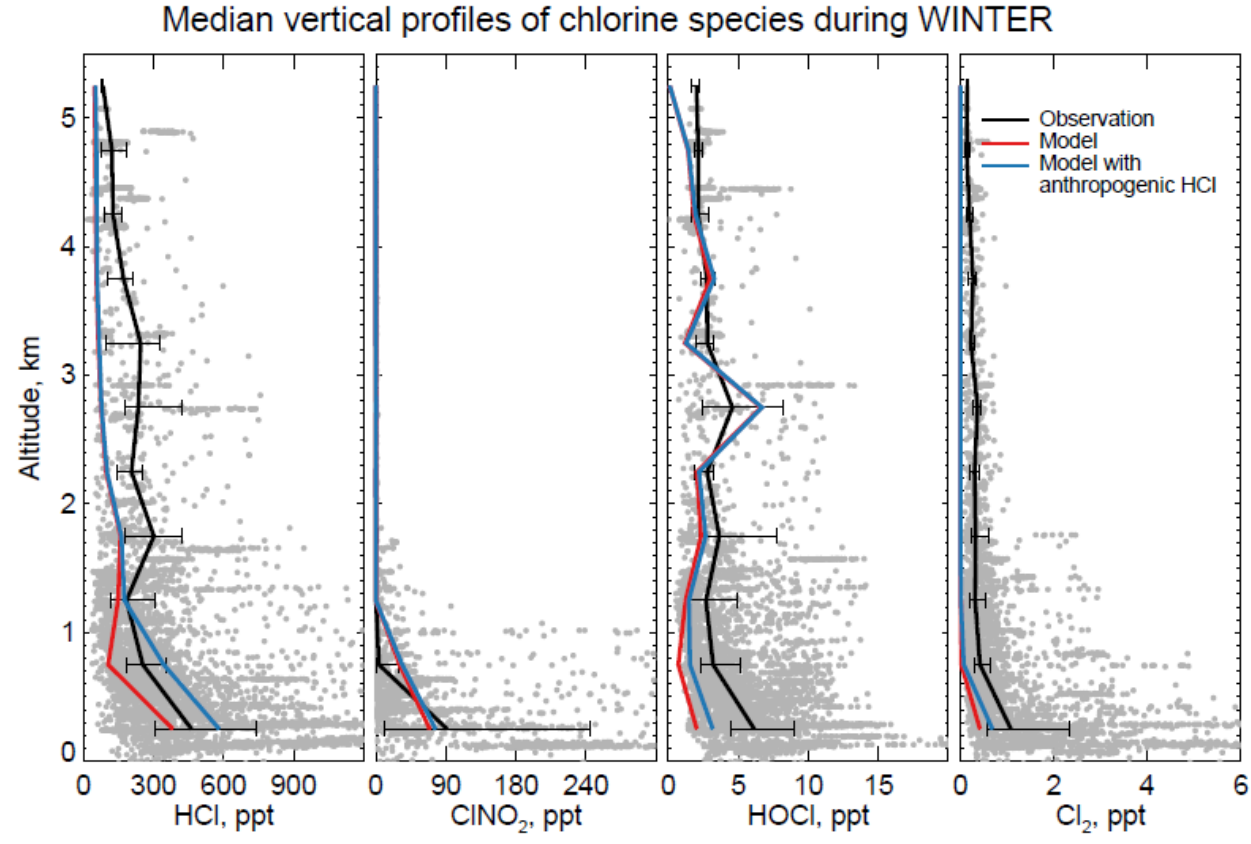

Figure 5: Vertical profiles of HCl, $ClNO_2$, HOCl, and Cl_2 mixing ratios during the WINTER campaign over the eastern US and offshore in February-March 2015. Observations from Haskins et al. (2018) are shown as individual 1-minute data points, with medians and 25th-75th percentiles in 500-m vertical bins. Measurements below the detection limit are treated as the median of 0 and detection limit. $ClNO_2$ data exclude daytime (10:00-16:00 local) when mixing ratios are near zero both in the observations and in the model (Figure 6). Model values are shown as medians sampled along the flight tracks. Also shown are results from sensitivity simulations including the anthropogenic chlorine inventory of McCulloch et al. (1999).

Atmos. Chem. Phys. Discuss., https://doi.org/10.5194/acp-2018-1088
Manuscript under review for journal Atmos. Chem. Phys.
Discussion started: 19 October 2018

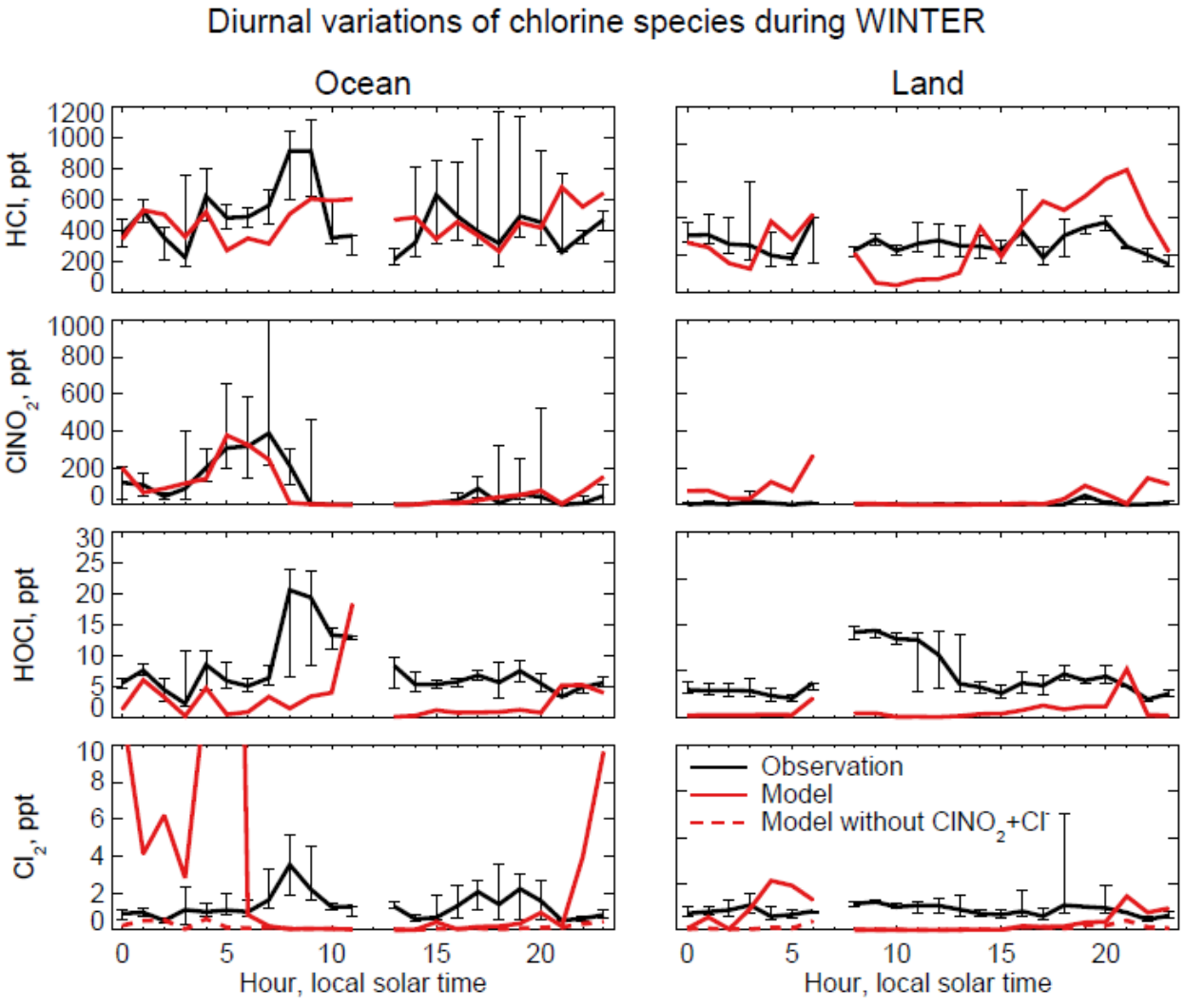

Figure 6: Median diurnal variations of HCl, $ClNO_2$, and Cl_2 mixing ratios below 1 km altitude during the WINTER aircraft campaign over the eastern US and offshore in February-March 2015. The data are separated between ocean (left panels) and land (right panels). Model values are compared to observations from Haskins et al. (2018). Vertical bars show the 25th-75th percentiles in the observations. Measurements below the detection limit are treated as the median of 0 and detection limit. Also shown are results from a sensitivity simulation excluding $ClNO_2$+Cl^-, which has negligible effect on HCl, $ClNO_2$, and HOCl, but brings the Cl_2 simulation in much better agreement with observations at night.

Atmos. Chem. Phys. Discuss., https://doi.org/10.5194/acp-2018-1088
Manuscript under review for journal Atmos. Chem. Phys.
Discussion started: 19 October 2018

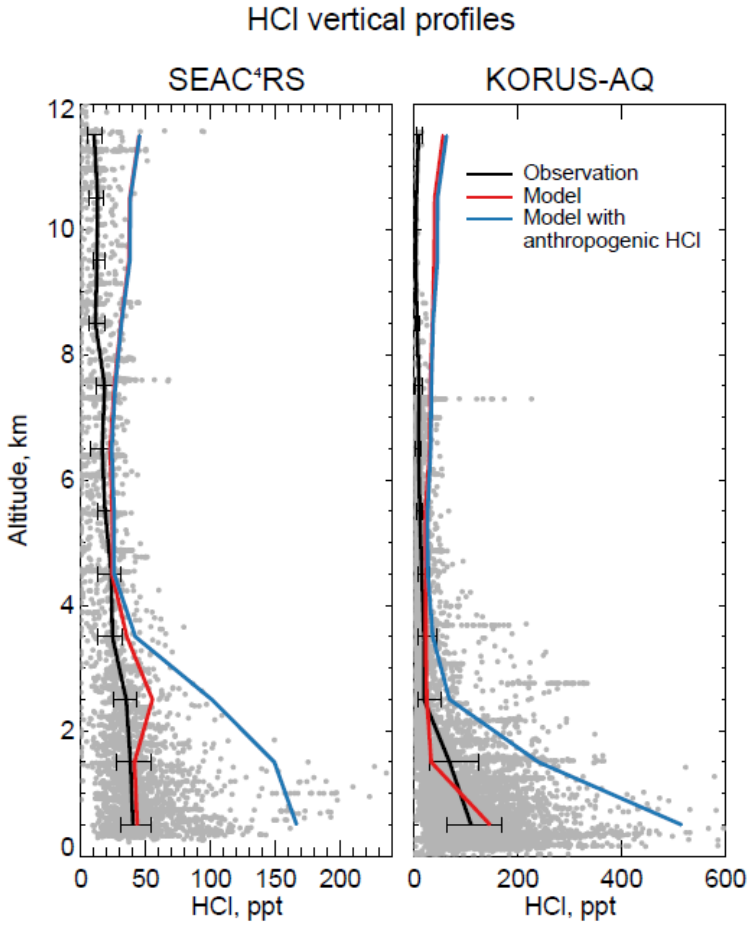

Figure 7: Vertical profiles of HCl mixing ratios during the SEAC⁴RS aircraft campaign over the Southeast US (95º-81.5°W, 30.5º-39°N) in August-September 2013 and during the KORUS-AQ aircraft campaign over and around the Korean peninsula (120º-132°E, 32°-38°N) in May-June 2015. Observations from the Georgia Tech CIMS instrument are shown as gray points (1-minute averages), with medians and 25th-75th percentiles in 1-km vertical bins. Model values are sampled along the flight tracks and for the measurement period. Measurements below the detection limit are treated as the median of 0 and detection limit.

Atmos. Chem. Phys. Discuss., https://doi.org/10.5194/acp-2018-1088
Manuscript under review for journal Atmos. Chem. Phys.
Discussion started: 19 October 2018

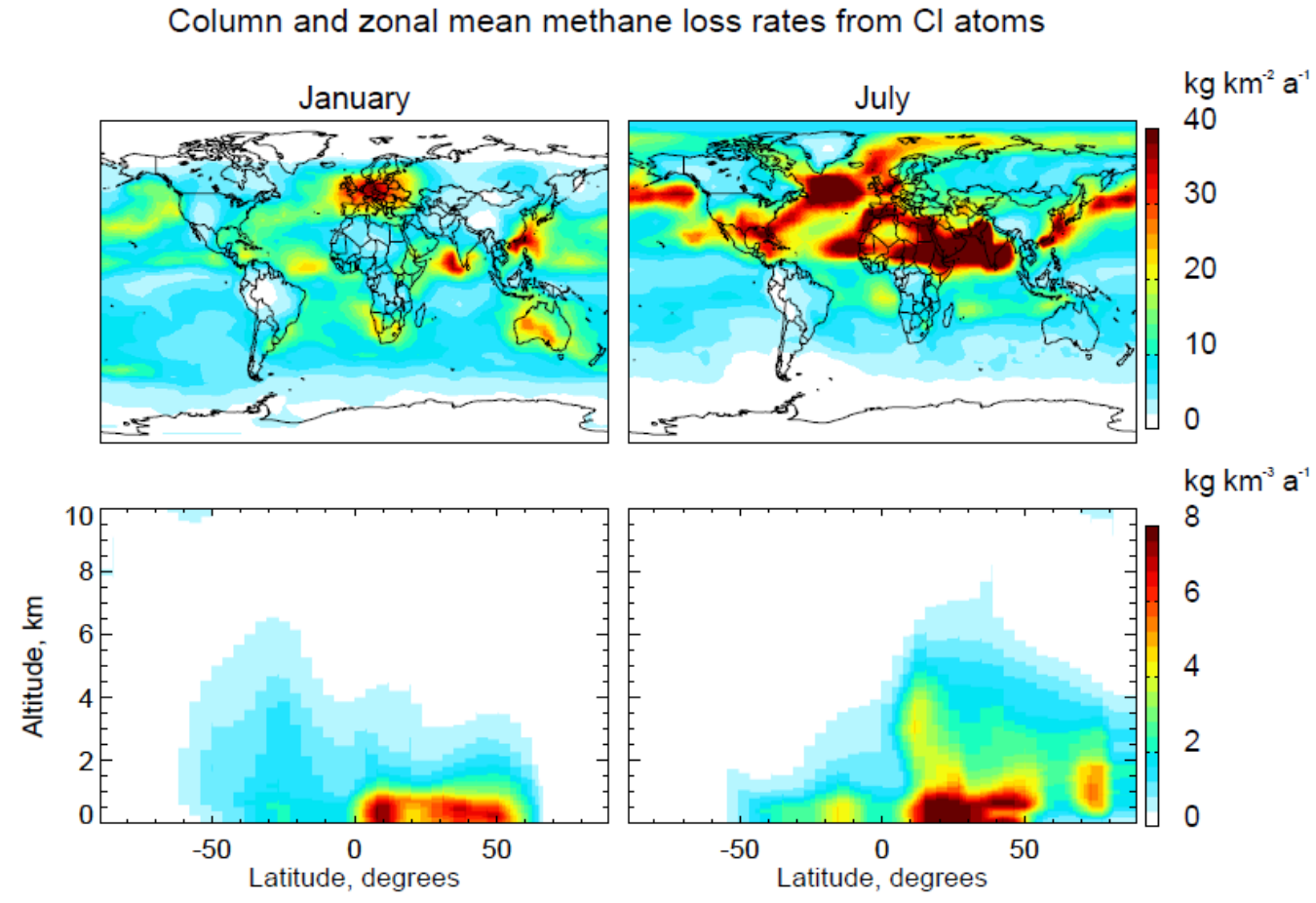

Figure 8: Global distribution of the methane loss rate from tropospheric oxidation by Cl atoms. Values are model monthly means in January and July. The top panels show the column-integrated loss rates in the troposphere and the bottom panels show the zonal mean loss rates as a function of latitude and altitude.

Atmos. Chem. Phys. Discuss., https://doi.org/10.5194/acp-2018-1088
Manuscript under review for journal Atmos. Chem. Phys.
Discussion started: 19 October 2018

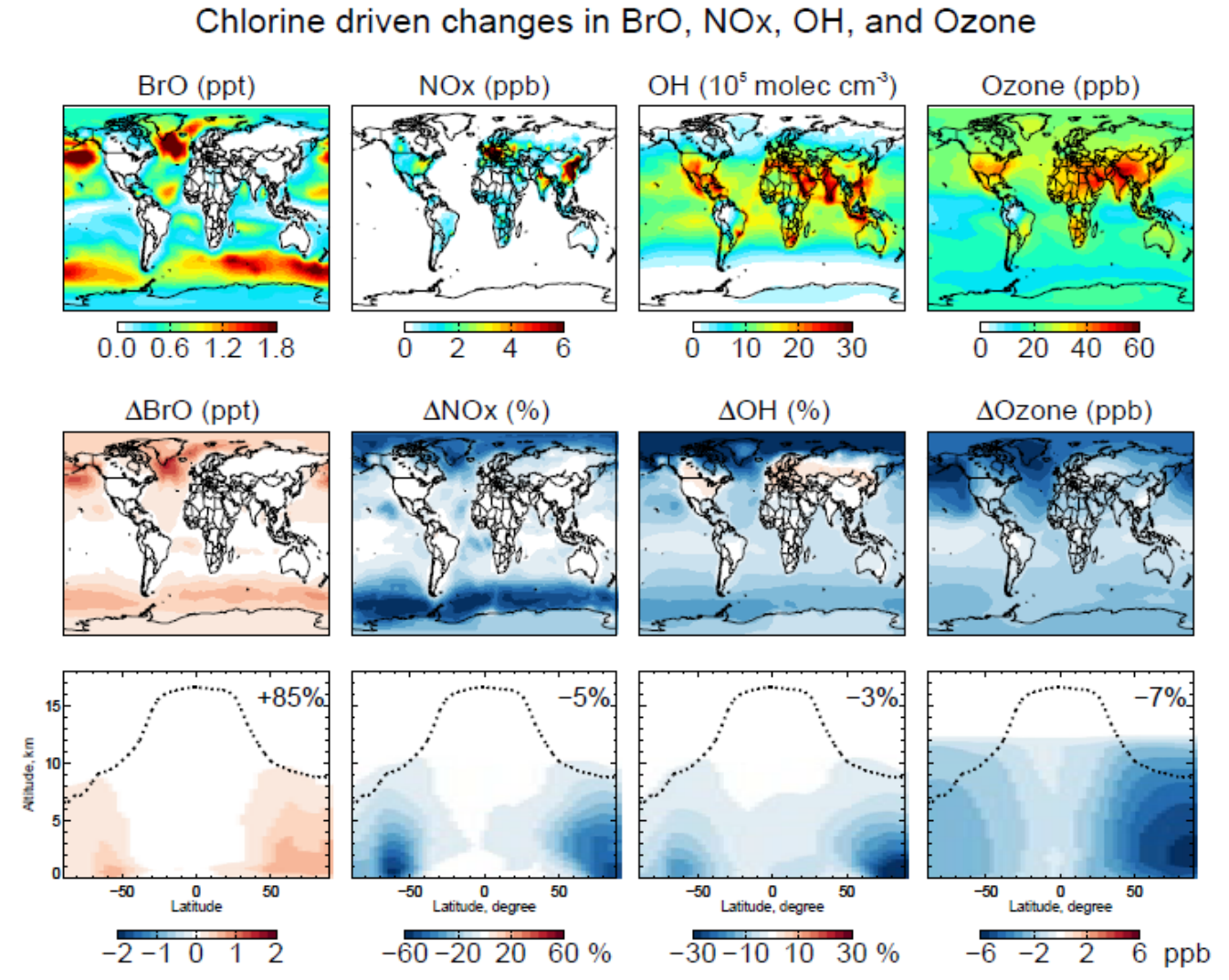

Figure 9: Effect of tropospheric chlorine chemistry on BrO, NO_x, OH, and ozone. The top panels show the annual mean surface mixing ratios of BrO, NOx, concentrations of OH, and mixing ratios of ozone simulated in our standard model including tropospheric chlorine chemistry. The lower panels show the changes in annual mean mixing ratios/concentrations due to tropospheric chlorine chemistry, as determined by difference with a sensitivity simulation including no Cl_y production and cycling. The middle panels show the changes in surface air mixing ratios/concentrations and the bottom panels show the changes in zonal mean mixing ratios/concentrations as a function of latitude and altitude. Black dashed lines indicate the tropopause. Numbers in bottom panels show the global tropospheric mean differences.